The Effects of Electronic Microscanning
on Infrared Image Aliasing and Spatial Resolution

by

Howard Jay Wexler

B.S.E.E., Tufts University College of Engineering, 1989

Submitted to the Department of Electrical Engineering and Computer Science
in partial fulfillment of the requirements for the degree of

Master of Science in Electrical Engineering and Computer Science

at the

Massachusetts Institute of Technology

May, 1995

Signature of Author: _____
Department of Electrical Engineering and Computer Science
May 12, 1995

Certified by: _____
Dr. William Clem Karl, Research Scientist
Laboratory for Information and Decision Systems
Thesis Supervisor

Certified by: _____
Thomas R. Briere, Manager of Detector Development
Raytheon Company, Electro-Optics Laboratory
Thesis Supervisor

Accepted by: _____
Frederic R. Morgenthaler, Chairman
Committee on Graduate Students

(This page intentionally left blank)

The Effects of Electronic Microscanning
in Infrared Image Aliasing and Spatial Resolution

by

Howard Jay Wexler

Submitted to the Department of Electrical Engineering and Computer Science
on May 12, 1995 in partial fulfillment of the requirements for the degree of
Master of Science in Electrical Engineering and Computer Science

ABSTRACT

Most modern infrared electro-optical imaging systems utilize staring imagers to acquire image data. Typical staring focal plane arrays contain a two-dimensional array of photodetectors. Each photodetector generates an electrical current or charge proportional to the number of photons striking its immediate vicinity. However, due to the discrete finite nature of the FPA detector lattice and fact that each photodetector's collection area is matched to the optical blur for signal to noise considerations, the imager does not satisfy the Nyquist criteria for sampling systems. Consequently, aliasing effects are usually an inherent part of images produced by staring arrays.

Microscanning is a method which can be used to reduce spatial frequency aliasing within an image by spatially oversampling the image scene. During the microscanning process, several optically dithered subimages are acquired and combined to create a larger image. The resulting image will have a higher sampling rate, and accordingly a greater Nyquist cutoff frequency, with the same spatial frequency resolution and optical cutoff frequency.

This thesis discusses the effects of a novel approach to the microscanning operation, called *electronic microscanning*. The electronic microscanning device performs the microscan operation by shifting the collection area of each pixel in the array by half-pixel increments instead of utilizing mechanical or liquid crystal filters to deflect the image. Electronic microscanning has an inherent advantage over traditional microscanning systems since no scanners or moving parts are needed to oversample the image. A model of the electronic microscan device is developed and compared to prototype laboratory results obtained at the Raytheon Company Electro-Optics Laboratory in Tewksbury, Massachusetts.

Thesis Supervisors:

Dr. William Clem Karl, Research Scientist, MIT Laboratory for Information and Decision Systems

Thomas Briere, Manager of Detector Development, Raytheon Company Electro-Optics Laboratory

(This page intentionally left blank)

Acknowledgments

First and foremost, I want to thank my wife Amy for her support during my return to the world of academia. It was Amy's belief in me that allowed me to believe in myself. I could not have done any of this without her love and wisdom. She deserves a medal for putting up with the endless study nights and problem sets, the irrational behavior around exam time, and the constant theft of Oreo cookies from her stash. ILY

Jerry is a friend and mentor who put his trust and belief in me, and I know that I have not let him down. I want to say thanks to him for taking me under his wing and giving me an opportunity of a lifetime.

Raytheon's Electro-Optics Lab would not be complete without Tom, who not only helped me fight the political battles, but also rolled up his sleeves to help in the laboratory, even when more urgent matters existed. Many thanks go to Tom for making all of this possible.

And it was Clem who went through the learning curve with me, forcing me to learn and understand everything that was going on. Thanks for accompanying me on this adventure.

There are countless others who helped me see the light, including (but certainly not limited to) Jim who had the vision for electronic microscan, Sergey who helped me understand the device physics, Karen and Rich who showed me the ropes at EOL, and Roger from who I borrowed tools, and who always knew where to find whatever I was looking for. And, a special hug goes to Rover for providing the perfect diversion when I needed a break from studying and for keeping Amy busy.

And last, but definitely not least, I want to express my sincere appreciation to my entire family for their support. I realize that these past few years I have been out of touch while pursuing my degree, but I know that this graduation makes everything worth it. I promise to visit much more often.

(This page intentionally left blank)

Table of Contents

(This page intentionally left blank)

1. Introduction

Most modern infrared electro-optical imaging systems utilize staring imagers to acquire image data. Typical staring focal plane arrays (FPAs) contain a two-dimensional array of photodetectors, each generating an electrical current or charge proportional to the number of photons striking its immediate vicinity. However, due to the discrete finite nature of the FPA detector lattice and the fact that each photodetector's collection area is matched to the optical blur for signal to noise considerations, the imager does not satisfy the Nyquist criteria for sampling systems. Consequently, aliasing effects are usually an inherent part of images produced by staring arrays.

Microscanning is a method which can be used to reduce frequency aliasing within an image by increasing the spatial sampling of the image. During the microscanning process, several optically dithered subimages are acquired and combined to create a larger image. The resulting image will have a higher sampling rate, and accordingly a greater Nyquist frequency, with the same spatial frequency resolution and optical cutoff frequency. This thesis discusses the effects of a novel approach to the microscanning operation, called *electronic microscanning*. Electronic microscanning has an inherent advantage over traditional microscanning systems since no scanners or moving parts are needed to oversample the image.

In order to have a better understanding of the impacts of the electronic microscanning process, it is essential to discuss the optical system through which the image is viewed, along with the method of collecting the electric charge created by the infrared photons. Once these systems are understood, the sampling event can be modeled. This thesis will compare the theoretical effects of the electronic microscanning device to actual laboratory results obtained with a prototype device. Finally, some of the system impacts and considerations will be discussed, along with suggestions for further research.

1.1 Optical Systems

The properties of optical systems have been studied in depth for centuries. Although not entirely linear, for our purposes an optical system can be thought of as a linear system. The input signal of this linear system is the light rays emanating from the viewed scene. The system function is determined by the optics and method of image acquisition, and the output of the linear system is the resulting collection of discrete values which are

commonly referred to as the pixels of the image. A number of excellent reference books exist which can provide the reader with a better understanding of optics. This discussion will consider only a handful of optical properties which impact the sampling of an image scene by a focal plane array imager.

As light rays pass through an aperture (i.e., as the rays pass into a lens), their direction, amplitude and phase are modified, just as water wavefronts propagating through an aperture do so in a radial manner. This phenomenon is known as *diffraction*, whose effects are a function of the light's wavelength and the diameter of the lens aperture. In the optical case, the lens aperture acts as a perfect circular boxcar lowpass filter. An ideal point source passing through this circular aperture will emerge as the two dimensional circular equivalent of the sinc function known as an Airy Disk, which is shown in Figure 1. The first zero of the Airy disk occurs at a radius of $1.22\lambda F/D$, where λ is the wavelength of light, F is the focal length of the lens, and D is the diameter of the lens. Therefore, the width of the Airy disk's mainlobe is $2.44\lambda F/D$. The mainlobe contains 84% of the point's power,[1] and the magnitude response falls off very rapidly as the distance from the center of the disk increases and can be considered as negligible. Consequently, the size of the Airy disk's mainlobe is often referred to as the size of the Airy disk.

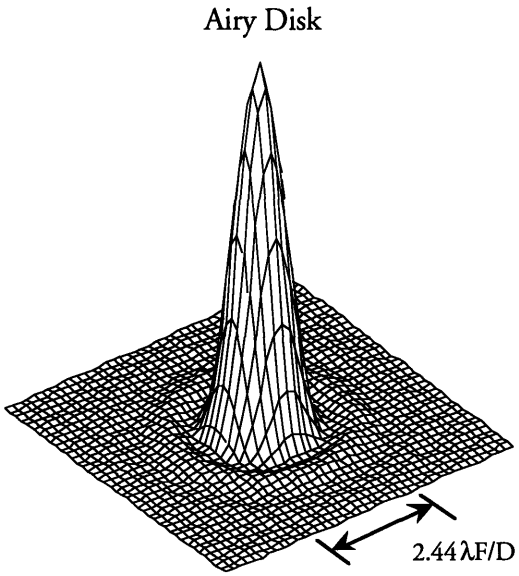

Figure 1. The Airy Disk is the two dimensional impulse response of a circular ideal lowpass filter (lens aperture).

[1] Spiro, p. 126.

When discussing the resolution of optical systems, it is more useful to refer to the *f/#* (pronounced 'f-number') of a lens instead of the ratio of the focal length to the diameter. The corresponding width of the Airy disk's mainlobe as a function of *f/#* is $2.44\lambda(f/\#)$.

In addition to diffraction effects, other optical imperfections (such as vignetting or misfocusing) may exist in a lens, which results in additional blurring of the input image and a corresponding widening of the diffraction Airy disk. For example, defocusing the image corresponds to convolving the input scene with a spatially symmetric lowpass filter. Aberrations in the lens will also contribute to the optical system function. Consequently, an ideal point source (impulse) will exit the lens system not as an Airy disk, but as a lowpassed version of the Airy disk called the *blur circle*. The diameter of this blur circle will be referred to as the *blur size*.

When assembling an imaging system, there are many tradeoffs which must be considered. The blur size, and therefore the best spatial resolution achievable at a given wavelength, is determined by the *f/#* of the lens. Lens cost is usually inversely proportional to the *f/#*. Integration time is inversely proportional to the square of the lens diameter.[2] For tactical infrared systems, sensitivity is frequently the most important consideration. In order to achieve maximum sensitivity, the optical system is matched to the detector array such that the blur size is equal to the detector size[3] as shown in Figure 2, which results in the best performance at the highest *f/#* possible. With this arrangement, a point source is imaged as a point by the focal plane array.

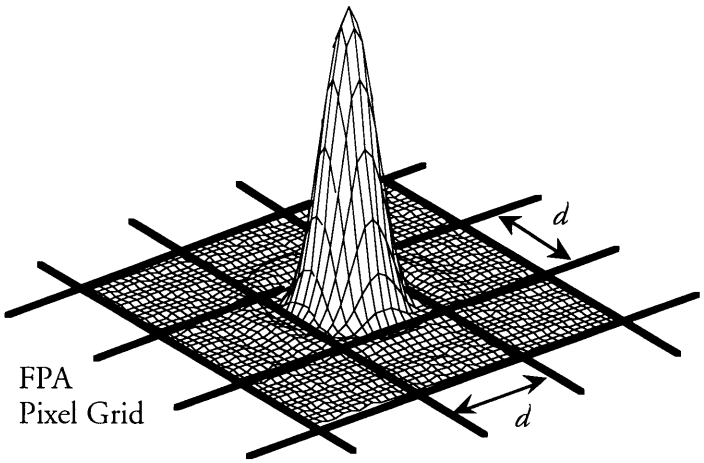

Figure 2. The diameter of the blur circle is matched to the detector size for maximum sensitivity. For this FPA, the detector area is d^2.

---

[2] Wildey, p.285
[3] Spiro, p. 127

For an example, consider a mid-wave infrared (MWIR) FPA sensitive in the 3–5μm band in which we wish to match the blur size with the detector size. If we have a detector element measuring 50μm square, for a diffraction-limited system we would need a lens with an *f/#* determined by:

$$f/\# = \frac{d}{2.44\lambda} = \frac{50\mu m}{(2.44)(5\mu m)} = 4.1 \quad (1)$$

With an imperfect optical system, one would reduce the diffraction-limited *f/#* requirement by 5 to 10% (depending on the quality of the optics), so that the ***blur*** size is 50μm.

1.2 Image Detectors

A proper understanding of the signal processing aspect of image acquisition requires knowledge of the device geometry and spatial response. Although there are a myriad of detector configurations and characteristics, this thesis will discuss those which are relevant to the relationship between the detector and the sampling of the image scene by the electronic microscanning device. The reader is referred to a reference book in semiconductor physics for further detail.

A hybrid infrared detector FPA consists of two primary components: the detector and the readout electronics (ROE). The detector consists of a doped material sensitive to the desired wavelength of light, which produces minority charge carriers in an amount proportional to the number of photons striking it. The detector array used in the electronic microscan device contains n-doped Cadmium-Telluride (CdTe) as its sensitive material, which produces electron hole (minority) charge carriers in response to absorbing light photons in the MWIR band. Attached to each detector in the array is a Mercury-Cadmium-Telluride (HgCdTe) p-n junction diode used to collect the minority charge carriers, and a capacitor to store the charge collected through the diode. The ROE provides a method of transferring the charge stored by the capacitors to an A/D converter in a convenient manner.

The minority charge carriers liberated by the photon travel in a random direction, contributing to the diffusion flow until being recombined with an electron, trapped along the semiconductor surface, or collected by an active diode. The ***diffusion length*** of the material is the average distance that a minority charge carrier travels before recombination and is a measure of the maximum collection radius of a photodiode.

The *fill factor* of a detector array is a measure of how much of the FPA (in percentage of area) is sensitive to light in the specified band. Insensitivities might exist for different reasons, such as the use of a portion of the substrate for the ROE or antiblooming barrier strips. The fill factor directly relates to the performance of the device, since a greater sensitive area will collect more photons and will more completely sample the input image scene. In order to maximize the useful sensitive area, many modern devices are using hybridized configurations as shown in Figure 3, in which the ROE is attached to the bottom of the substrate through conductive pads known as *bumps*, achieving virtually 100% fill. The electronic microscan device uses this method.

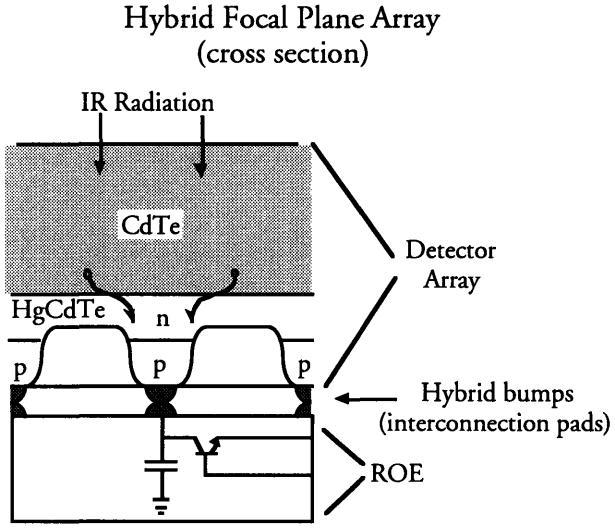

Figure 3. The Hybrid FPA consists of two parts sandwiched together. The *detector array* contains the IR-sensitive material which generates the minority charge carriers and the photodiode used to collect the carriers. The detector array connects to the *read-out electronics* (ROE) via indium interconnection pads (bumps). This arrangement virtually has a 100% sensitive area (fill factor).

In addition to the fill factor, each detector has a geometric sensitivity pattern or collection area function. Due to the random nature of minority charge carrier travel, in a tightly packed array of detectors (in which the detector spacing is less than the diffusion length of the material) photons which land on the border between two detector diodes have an equal probability of contributing to the current passed through either diode. Consequently, the detector weighting function or *geometric collection area* of a typical detector is in general not uniform, but tapered at the edges as shown in Figure 4. For modeling purposes, the collection area will be approximated as a boxcar function with no crosstalk between adjacent cells.

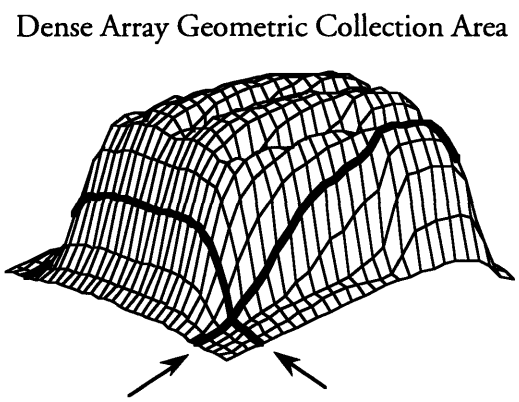

Figure 4. In a densely-packed array (where the pixel pitch is less than the diffusion length), typical 100% fill factor detectors have a collection area that is close to a two-dimensional boxcar function. This is a graph of the collection function for an actual photodetector from a typical array. The geometry of the detector collection function directly impacts the spatial frequency response of the array.

If the array is sparse, such as when detector spacing exceeds the diffusion length of the material, the minority charge carriers liberated near the periphery have a much higher chance of recombining with electrons and not contributing to the diffusion current. Consequently the collection area will appear to be more bell-shaped and dependent on the diffusion length.

1.3 Image Sampling Theory

An infrared electro-optical imaging system consisting of telescope lenses and a detector assembly is used to sample an infrared scene, and is consequently governed by the rules of sampling theory. Although not completely linear,[4] the imaging system (and each component within) is modeled as a linear system.[5] In this system, a continuous two-dimensional signal (the scene) is lowpass filtered by the optical telescope. Each photodetector within the array integrates the filtered image over a local finite area and samples the result. Negligible effects, such as semiconductor charge transfer inefficiencies and diffusion phenomenon will be ignored in this model. In order to more easily understand the two dimensional operations, the one dimensional equivalents will be discussed, and subsequently expanded into the second dimension.

---

[4] Wittenstein et. al., p. 41
[5] Horn, p. 104

Linear shift invariant (LSI) systems can be uniquely described by their impulse response.[6] Each component within the optical system has its own system function which contributes to the overall response. The output of each component is the convolution of the input with the component's system function, which has the corresponding property of a multiplication in the spatial frequency domain.

The optics behave as an ideal lowpass filter as a result of having a finite aperture with a cutoff frequency (at a given wavelength) determined by the *fl#*. Consequently, no spatial frequencies higher than the optical cutoff frequency are allowed to propagate through the system. In the spatial domain the impulse response of the ideal lowpass filter is the Airy Disk discussed earlier. For our one-dimensional analysis, the ideal lowpass filter with a cutoff frequency ω_c yields an impulse response of the sinc $\left(\frac{\sin(x)}{x}\right)$ function. According to the Nyquist sampling theorem, the resulting signal must be sampled at twice the cutoff frequency in order to prevent frequency aliasing.

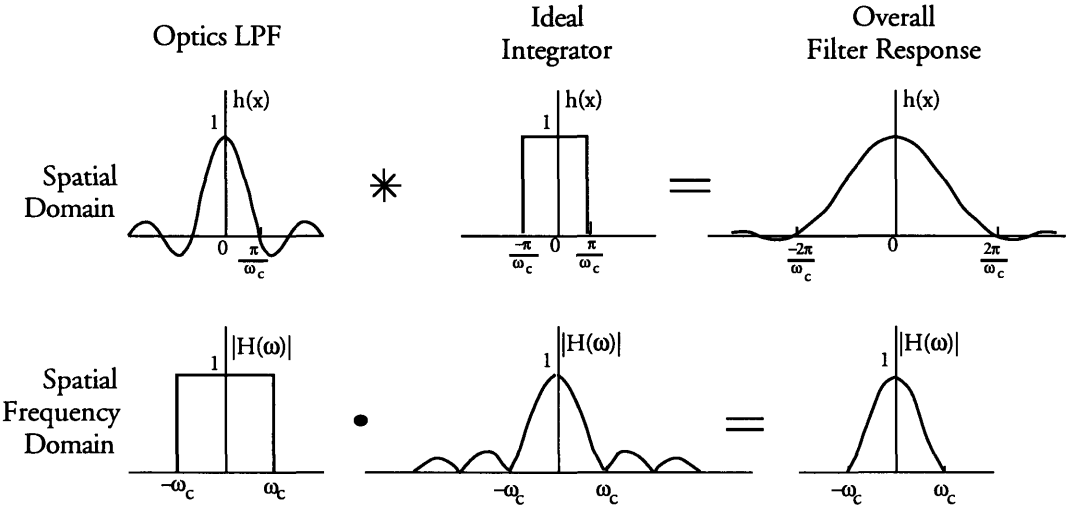

Figure 5. The frequency response after lowpass filtering and integrating with an ideal boxcar is a truncated sinc function.

The detectors perform two functions: integration and sampling. As an integrator, the detector convolves the input signal with a geometric collection function which is determined by the detector device physics and geometric layout. Assuming a boxcar integration function matched to the lowpass filter, in the frequency domain the input is multiplied by a sinc function whose first zero crossing is at the cutoff frequency of the

[6] Oppenheim, p. 21

lowpass filter. The overall filter response of the ideal lowpass filter and integrator is shown in Figure 5.

The detectors also sample the signal. Unfortunately, the filtered signal is sampled at a frequency equal to its cutoff frequency (as determined by the optics) rather than at twice the cutoff frequency. Due to the sampling replication effect in the frequency domain, aliasing will result for any frequencies in the upper half of the passband. The result can be seen in Figure 6.

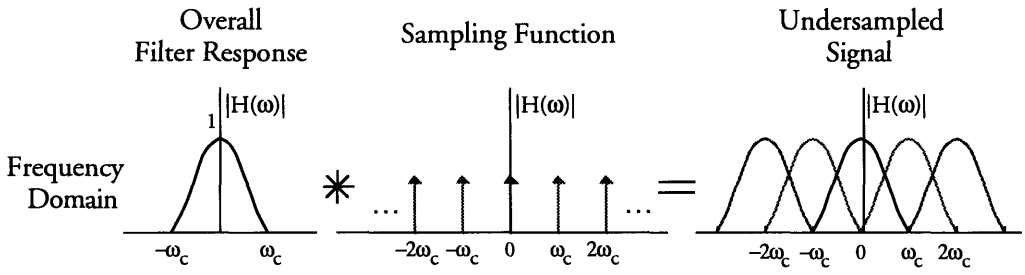

Figure 6. Aliasing (in the spatial frequency domain) is the result of sampling the signal at its cutoff frequency.

Expanding to the second dimension, the discrete-time output $o[m,n]$ of the imaging system in response to a continuous time input signal $i(x,y)$ can be represented mathematically by the following equation:

$$o[m,n] = \sum_{m=0}^{N-1}\sum_{n=0}^{N-1}\big(r(x,y)*h(x,y)*i(x,y)\big)\delta[x-md, y-nd] \qquad (2)$$

where $r(x,y)$ is the geometric collection transfer function, $h(x,y)$ is the system function of the optics, N is the number of detectors in the square array, d is the width of the square detector and detector spacing (assuming a 100% fill factor), and $\delta[x,y]$ is the two dimensional dirac delta function. For notational simplicity, normalization constants have been omitted from (2).

Since the imaging system is noncoherent, we are interested in the magnitude response of the system. The modulation transfer function (MTF) is a performance measure describing the magnitude response of the system to inputs of varying spatial frequencies.[7] Specifically, the MTF is a measure of contrast gain of the system, and is

[7] Bradley et al. (1987), pp. 33-34

defined as the normalized difference between the maximum and minimum values returned for a binary image at a given spatial frequency, as defined by the equation:

$$\text{MTF} = \frac{\text{Max} - \text{Min}}{\text{Max} + \text{Min}} \tag{3}$$

where Max is the maximum value returned by the system, and Min is the minimum value returned.

The discussion so far has assumed that the optics behave like a linear shift invariant system. Unfortunately, FPAs can exhibit nonisoplanatic effects, or a changing response to differing phases of a stable input signal. For an example of the nonisoplanatic effect, consider an image of two binary (black and white) bars of energy magnitude = 2, which are one pixel wide, and happen to be two pixels apart. A one-dimensional sampled version of that image might be represented by the sequence: [...000202000...] However, if the image is shifted by half a pixel such that the sampling points are not centered on the bars, the bars becomes blurred, and the energy is spread among the surrounding pixels, resulting in the sequence: [...0001111000...], as shown in Figure 7. If the deflection is not exactly one-half pixel, then the individual bars can still be detected, but the peak amplitude and contrast in the image has been significantly reduced. This can more easily be seen by viewing a repetitive pattern (such as a fence) through the imager, which may appear binary at points, and gray at others.

The MTF curve of the 100% fill factor FPA imaging system as a function of input frequency is shown in Figure 8a, and as a function of output frequency in Figure 8b. The solid lines correspond to the maximum (totally in phase) response, representing the relative maximum contrast observable by the system in response to an input at the given spatial frequency. These curves have a second dotted line which represents the minimum MTF at each frequency due to the nonisoplanatic effects. Because the system is undersampled, as the input frequency passes the system's Nyquist frequency in Figure 8b, aliasing occurs as indicated where the line changes direction and the perceived frequency decreases as the input frequency increases.

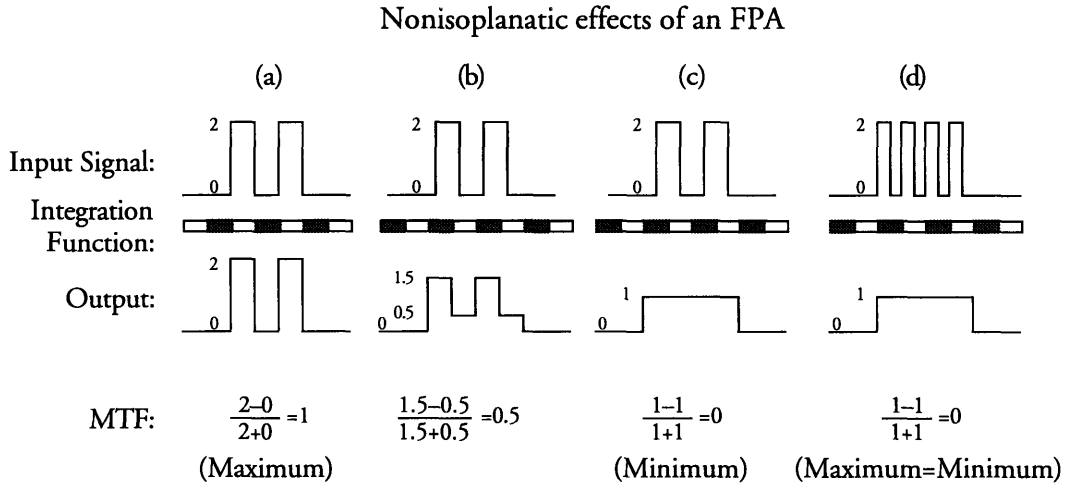

Figure 7. Depending upon the phase of the sampling system relative to the input, a signal can be interpreted in different ways. These differences are an example of phase-dependent, or *nonisoplanatic* effects. Figures (a), (b), and (c) show how a binary input signal whose bar width corresponds to the sampling interval can have an MTF ranging from a maximum of 1 to a minimum of 0. Figure (d) reveals that a binary input with a bar width equal to half the sampling interval will have an MTF of zero regardless of the phase relationship.

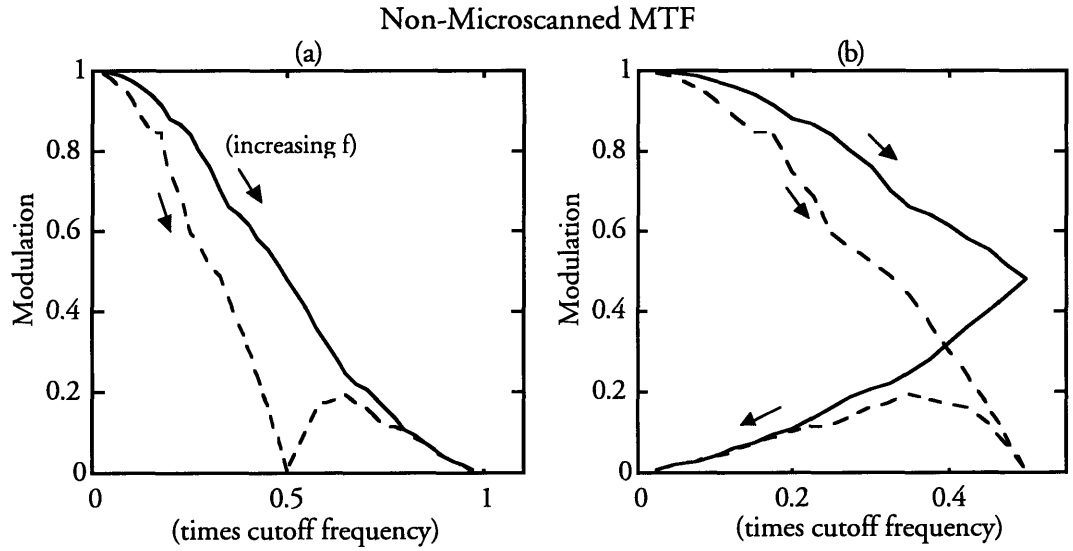

Figure 8. The Modulation Transfer Function of an undersampled system (a) as a function of input frequency, and (b) as a function of (perceived) output frequency. The input frequency increases from zero to the cutoff frequency as the lines progress from the upper left hand corner. As the input frequency passes the Nyquist frequency the system begins to alias, and the perceived frequency decreases toward zero. The solid line represents the maximum contrast observable at a given input frequency, and the dotted line the minimum.

2. Microscanning

Aliasing in the undersampled system can be eliminated through the oversampling technique known as microscanning. In one dimension, microscanning is analogous to double-sampling the input signal with two integrator/samplers which are 180° out of phase with each other, and recombining the samples to create an oversampled (by a factor of two) output, as shown in Figure 9. In this case, the Nyquist frequency has doubled due to the extra sampling, but the frequency resolution remains the same since the integration function has not changed. The MTF for a 2× microscanned system is shown in Figure 10, which also shows that nonisoplanatic effects are reduced by microscanning[8] as evident by the reduced disparity between the minimum and maximum MTF curves. Also note that aliasing has been eliminated.

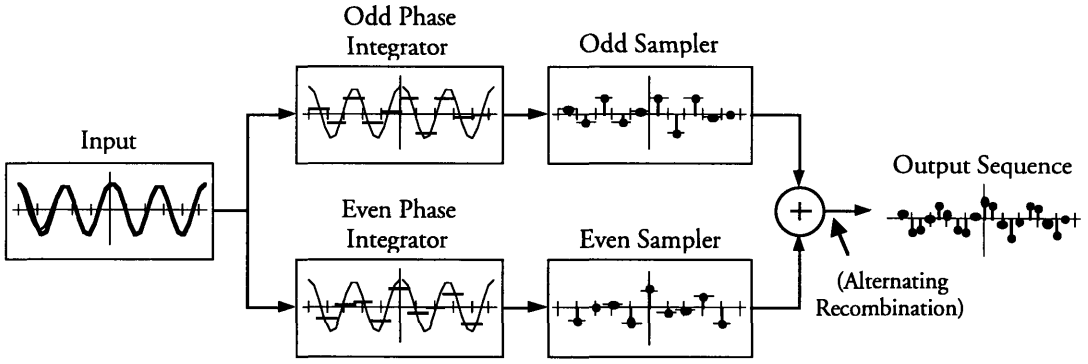

Figure 9. Microscanning is analogous to oversampling with two integrator-samplers operating 180° out of phase with each other. The outputs of each sampler are recombined to create a signal with twice as many data points.

In an imaging system, microscanning can be achieved in a similar manner. Supposing we have an $N \times N$ detector array, in order to create a 2×2 microscanned image, the scene is captured four times in the following manner: the first $N \times N$ subimage is taken at a reference position. The second subimage is captured with a deflection of the scene in the x direction by one-half pixel. The third subimage is deflected by one-half pixel in the y direction relative to the reference position. The fourth subimage has a one-half pixel deflection in both the x and y directions relative to the reference. The four subimages are recombined to create a composite image of the scene which has been sampled at a more frequent interval and is composed of $2N \times 2N$ pixels, as shown in Figure 11.

[8] Dann et al., p. 125

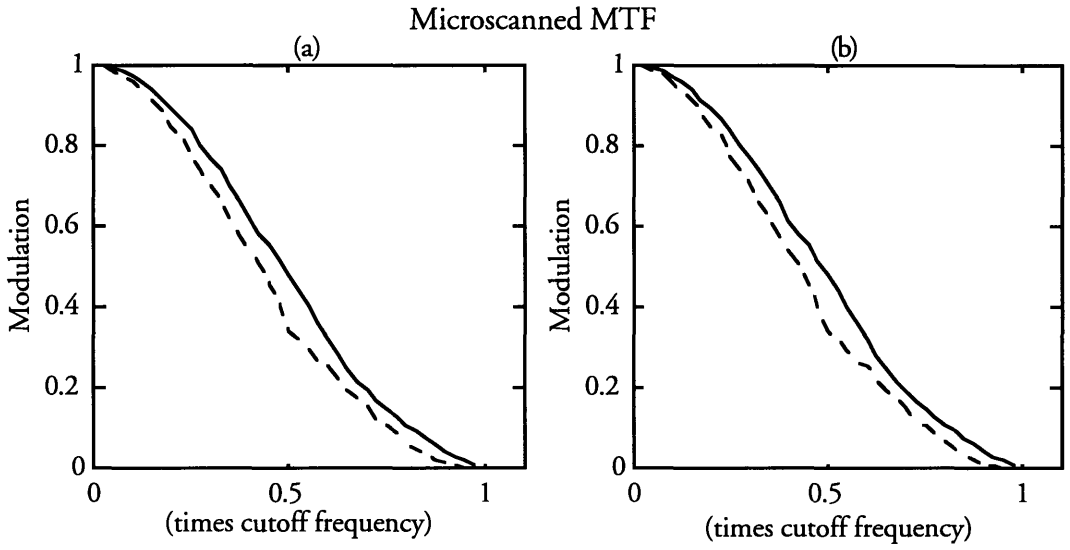

Figure 10. The MTF of a 2× microscanned system (a) as a function of input frequency, (b) as a function of (perceived) output frequency. Compared to the non-microscanned system in Figure 8, nonisoplanatic effects are reduced (shown by the reduced disparity between the solid and dotted lines) and the Nyquist frequency is doubled in the 2× microscanned system, resulting in no aliasing.

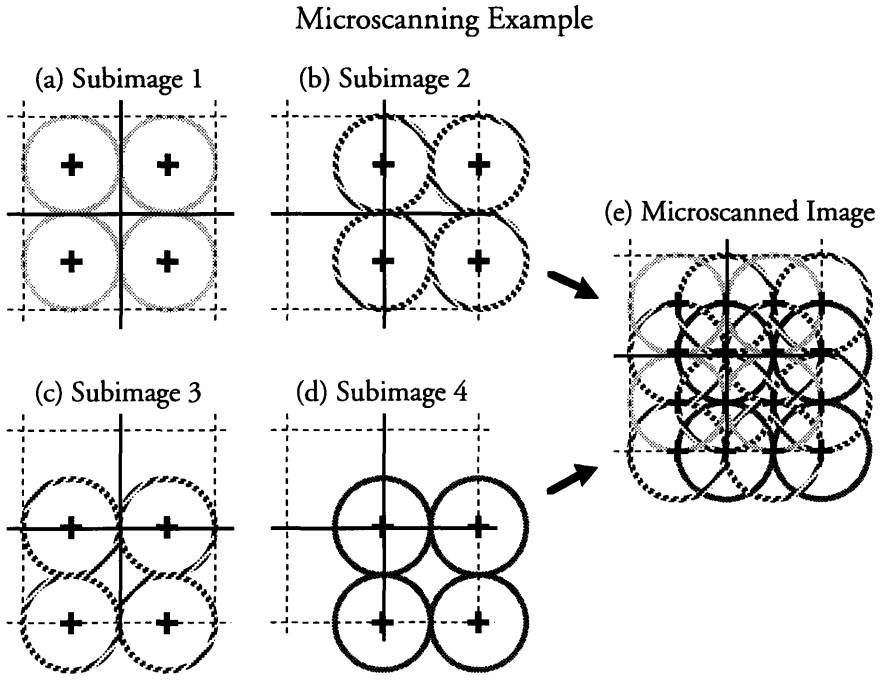

Figure 11. An example of microscanning. Four subimages (a, b, c, and d) are collected. The subimages are recombined to create a composite (e) with twice as many data points in the x and y directions.

Mathematically, the microscanned image $u[m,n]$ is defined by the following equation:

$$u[m,n] = \sum_{n=0}^{N-1}\sum_{m=0}^{N-1}\left(r(x,y)*h(x,y)*i(x,y)\right)\cdot\begin{pmatrix}\delta[x-md,\,y-nd]\\ +\delta[x-(m+\frac{1}{2})d,\,y-nd]\\ +\delta[x-md,\,y-(n+\frac{1}{2})d]\\ +\delta[x-(m+\frac{1}{2})d,\,y-(n+\frac{1}{2})d]\end{pmatrix}$$

$$= \sum_{n=0}^{2N-1}\sum_{m=0}^{2N-1}\left(r(x,y)*h(x,y)*i(x,y)\right)\cdot\delta\left[x-\frac{md}{2},\,y-\frac{nd}{2}\right] \qquad (4)$$

In essence, the system is being sampled at twice the original sampling frequency, with a corresponding increase in the Nyquist frequency, and with the same collection function. Therefore, the nonaliasing criteria for our bandlimited input signal has been met. Unfortunately, this comes at the price of a decrease in integration time by a factor of four (since four subimages must be collected at the same frame rate) and an increase in the signal processing needed (due to the larger number of pixels in the image).

2.1 Electromechanical Microscanning

Several methods have been developed to implement the microscan process. The different methods which have been documented basically fall into two groups: deflection of the line of sight through electromechanical devices that have optical elements, and shifting of the light rays using liquid crystal beam steerers. Each of these methods manipulate the optical line of sight in order to implement microscanning. Data processing recombines the subframes to form the microscanned image. Unless concurrent imaging is performed, the frame rate for the system is reduced by a factor of four since the FPA must be read four times to create one image frame.

The microscanning process can be performed by deflecting the optical line of sight with electromechanical devices. For this type of system, the fixed optical lenses are supplemented by a microscanning optical filter comprised of mirrors, prisms, or additional lenses which adjust the system's line of sight. An example of a mirror microscanning filter system is shown in Figure 12. The microscanning filter is driven by galvanometric motors or piezoelectric devices, and are stepped in half pixel increments in the required square pattern between subframes.

Sample Electromechanical Microscanning System

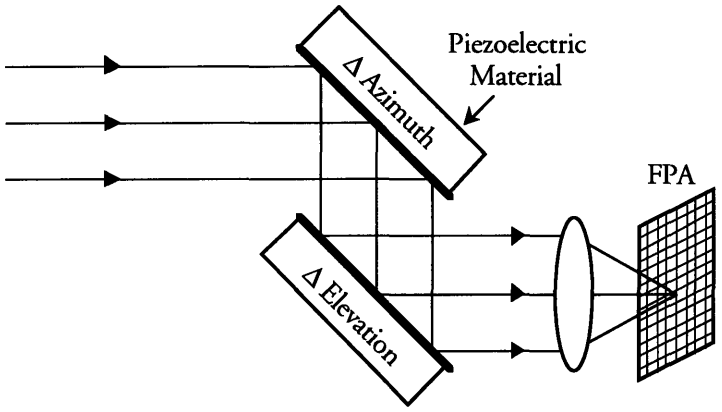

Figure 12. By using electromechanical components to deflect the scene, microscanning can be implemented in a simple manner.

When choosing an actuator for an electromechanical system, one must consider the different tradeoffs of size, weight, stability and deflection angle. In general, galvanometers are heavy and bulky but can handle wide ranges of motion and heavier loads. In comparison, piezoelectric materials are smaller and lightweight but have a limited range of motion (which might be acceptable for microscanning systems), but may be unstable (i.e. bimorph piezoelectrics).[9]

Electromechanically-based systems have the disadvantage that the additional actuators and optics take up a considerable amount of real estate and weight in the imaging system while adding another dimension of complexity (i.e. servo loops, position-sensing devices, timing generators and driver circuits). In addition, the benefits of the microscanning process are limited by inaccuracies in the electromechanical positioning system, which must undergo a calibration process.[10] Electromechanical devices usually require large currents, and are often operated at their mechanical limits due to the operational requirements of the microscanning system. Additional delays must be added between subimages to compensate for repositioning the microscan mirror and settling of transients.

2.2 Nonmechanical Microscanning - Liquid Crystal Beam Steerers

More recently, the use of liquid crystal (LC) optical beam steerers has been researched and developed to implement microscanning. LC beam steerers (also known as optical space-fed phased arrays) are analogous to phased array radar systems in that the

[9] Awamoto, pp. 214-215
[10] Lenz and Lenz, p. 108

optical rays are redirected by electronical means. Although it is still in its maturing stages, LC technology provides an attractive alternative to electromechanical methods due to less complexity and real estate demands required by the LC systems.

Common LC materials are transmissive in the visible and infrared bands. Consequently, their optical properties have been the focus of much recent research. It has been discovered that there is a fairly linear relationship between A.C. voltage differential and optical deflection in the unsaturated transition region of operation of LC materials.

An LC filter used for microscanning is actually composed of two electro-optical liquid crystal arrays several microns thick, polarized in orthogonal directions and sandwiched together, separated by two transparent substrates. Each cell in the array has an independent voltage source which is used to control the index of refraction of the material, and induces an optical phase deflection for rays passing through that LC filter element. The composite filter array is placed between the imager optics and the FPA, as shown in Figure 13. Similar to the electromechanical method, four subframes are collected, with an appropriate voltage function change between subframes to accomplish the box deflection pattern.

Sample LC Microscanning System

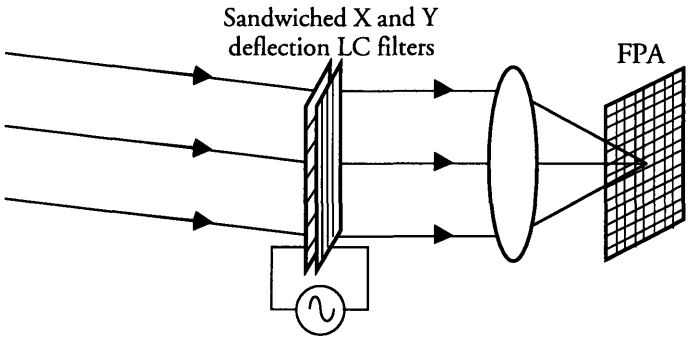

Figure 13. LC Filters can be used to achieve microscanning while reducing the size and complexity of the hardware needed. However, present LC materials have very slow response times.

LC filters occupy much less space than their electromechanical counterparts. Consequently, savings are realized due to real estate economy. In addition, since there are no moving parts and the response of the LC array does not degrade over time, the LC technology provides a simple, repeatably accurate solution. However, LC filters have very

slow response times[11] which severely limit their application to non-time critical solutions. However, the technology is still in its infancy, and might prove fruitious as it matures.

2.3 Electronic Microscanning

Instead of deflecting the optical subassembly to create the half-pixel dithering, what if one were able to shift the sensitive area of the FPA by half-pixel increments? Such a device could revolutionize microscanning system design. Additional optical LC filters or heavy electromechanical subassemblies would no longer be needed to achieve the proper Nyquist sampling rate of the input image. Irregularities due to optics vibration or uncalibrated motion would be eliminated. This is the motivation behind electronic microscanning.

[11] McManamon et al., 1993a, p. 2657

3. Electronic Microscan Device

An electronic microscan device has been developed by the Raytheon Company Electro-Optics Laboratory. The proof-of-concept prototype was designed by Jim Wey of Raytheon's Research Division in Lexington, Massachusetts.

3.1 Electronic Microscan Device - Design

The electronic microscan FPA is a Mercury-Cadmium-Telluride (HgCdTe) infrared detector with 128×128 unit cells, which creates a 256×256 microscanned image. The device is sensitive in the 3μm to 5μm wavelength infrared band. Based on a rolling readout design, column shift registers distribute the integration, reset, and select signals to each pixel. Row shift registers handle the integration capacitor discharge and charge transfer signals. Similar to the methods discussed earlier, four 128×128 subimages per 256×256 image are collected from the electronic microscan FPA.

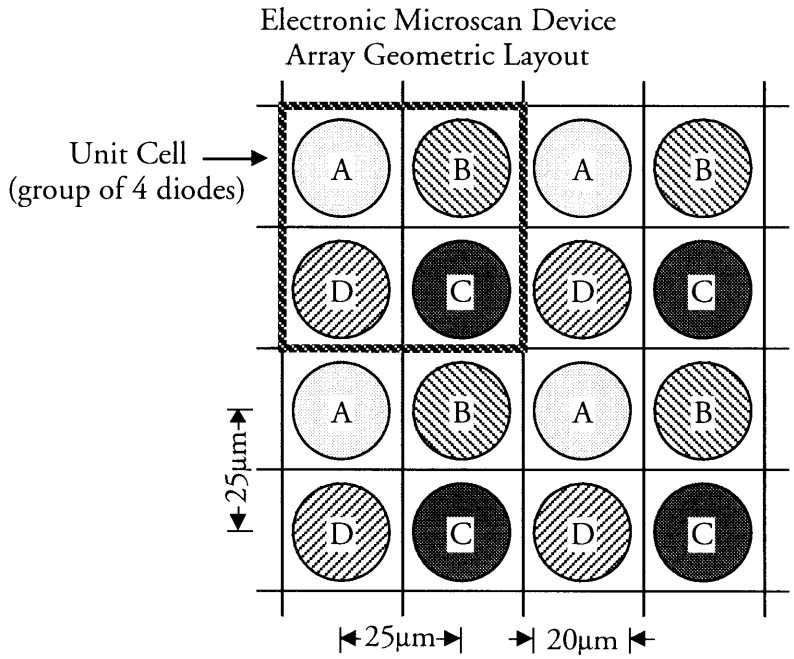

Figure 14. Geometric layout of the device at the unit cell level. 20μm circular photodiodes are arranged in a square. During a given subframe, only photodiodes of one type (A, B, C, or D) are active. The remaining photodiodes are floating and do not collect liberated minority charge carriers.

The read-out electronics (ROE) perform the microscan function. Each ROE unit cell contains four 20μm circular photodiodes arranged in a square, as shown in Figure 14. The photodiode spacing is 25μm in the x and y directions. During microscan operation,

one of the four photodiodes is active for a given subframe, and the remaining three are left floating. A different photodiode is selected for the subsequent subframe. All of the unit cells in the array are synchronized such that the individual unit cells select the active photodiode in a clockwise pattern.

Since an active photodiode in the electronic microscan FPA is surrounded by inactive floating photodiodes, the collection area for the active photodiode is limited by the diffusion in the HgCdTe material. Accordingly, the expected pixel collection area should be Gaussian-like and is predicted to have a diameter on the order of 40μm, which creates an overlapping sampling function.

3.2 Electronic Microscanning Device - Sampling Theory

There are several items to consider when determining the MTF of the electronic microscan device. Of primary importance is the collection area of each pixel. As determined earlier, a completely overlapping rectangular collection function ideally samples the optically bandlimited input signal. However, it is estimated that the electronic microscan device will have a Gaussian-like (but not Gaussian) distribution. Although it will not be the optimal oversampler, due to the overlapping pixel collection areas, aliasing and nonisoplanatic effects will be reduced by the electronic microscan device.

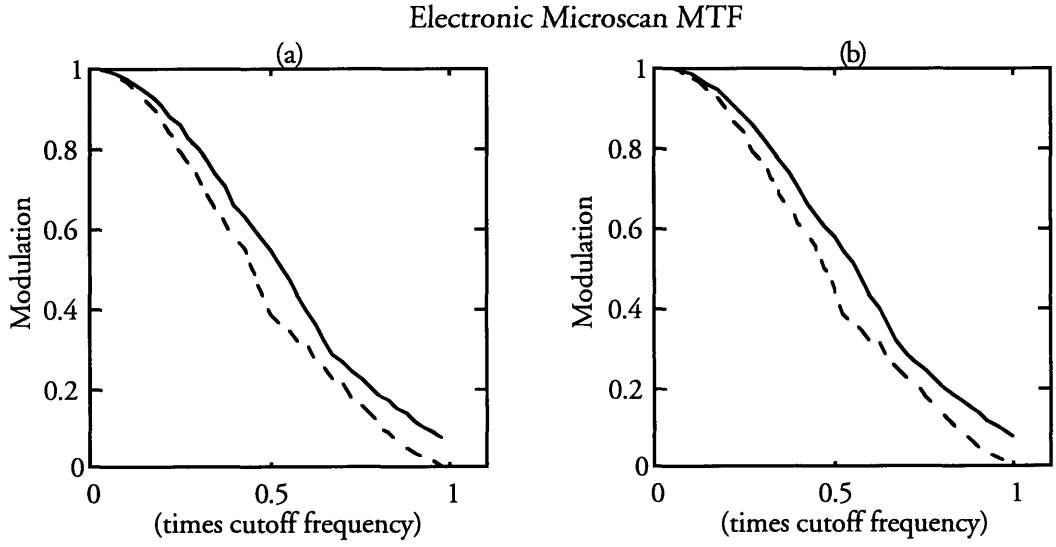

Figure 15. The MTF of the electronic microscan model shows the elimination of signal aliasing and the reduction of the nonisoplanatic effects. This model assumes a Gaussian-like collection area on the order of 40μm, a 50μm Airy disk, and a sampling pitch of 25μm. (a) is a graph of MTF as a function of input frequency, and (b) is a function of output frequency.

Figure 15 shows the MTF for the one dimensional electronic microscan device model, which assumes a bell-shaped response with the 50% point at a radius of 40μm. Also assumed is an optical system which yields a 50μm Airy disk, with no additional optical defects.

There are four interesting configurations which are obtained by changing the sampling collection area and blur size. The first is a non-microscanned 128×128 image with a 50μm pixel and blur size and 50μm sampling pitch, which represents a typical non-microscanned image and is the baseline to which the electronic microscan device is compared. To obtain this image, only one of the four electronically microscanned subimages are used. Herein this will be referred to as the *128×128 non-microscanned* configuration. Figure 16 shows the basic system spatial frequency domain response of the one dimensional model of the 128×128 non-microscanned configuration.

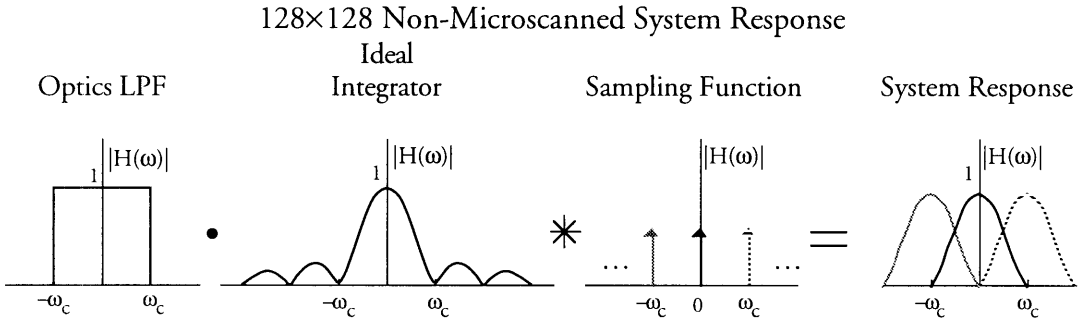

Figure 16. Spatial frequency domain system response for the one dimensional model of the 128×128 non-microscanned system. A 50μm blur is integrated by a 50μm pixel and sampled at a 50μm pitch, resulting in aliased frequencies.

If a 128×128 50μm array were used in a typical electromechanical microscanning system, the result would be a 256×256 microscanned 50μm pixel and blur size with a 25μm sampling pitch as discussed earlier. With the electronic microscan device, this configuration is obtained by recombining the four subimages as shown in Figure 11, and is called the *256×256 microscanned* configuration. The response of the one dimensional model is shown in Figure 17.

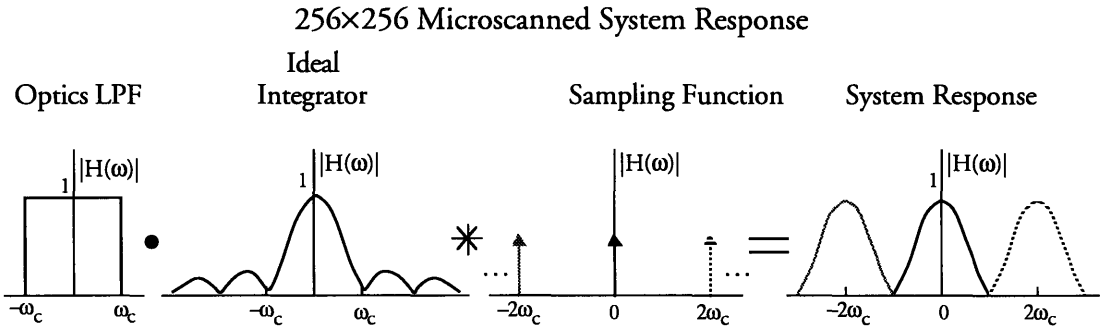

Figure 17. Spatial frequency domain system function for the one dimensional model of the 256×256 microscanned system. A 50μm blur is integrated by a 50μm pixel and sampled at a 25μm pitch, resulting in no aliased frequencies.

If the surrounding inactive pixels are grounded on the electronic microscan device (essentially making them active), the collection area of the active pixels is redefined to be 25μm square since the active photodiode spacing is less than the diffusion length of the material. Consequently, one can also obtain a *256×256 oversampled* image with the electronic microscan device. In this case, the 50μm optical blur is being properly sampled at a 25μm pitch. Figure 18 shows the spatial frequency domain response for this system.

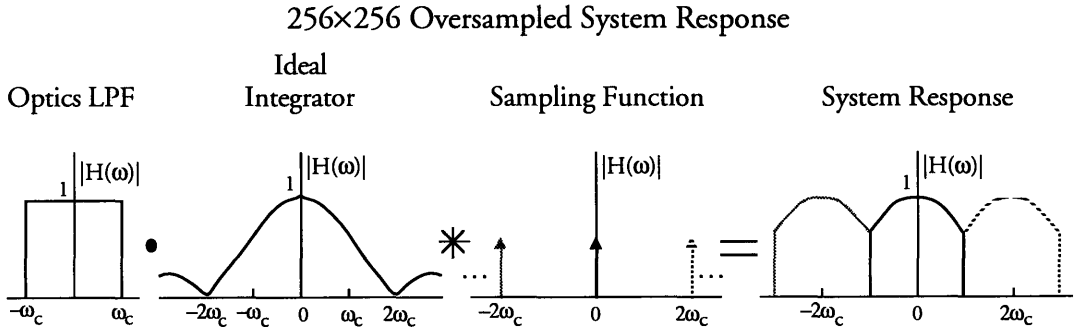

Figure 18. Spatial frequency domain system function for the one dimensional model of the 256×256 oversampled system. A 50 μm blur is integrated by a 25μm pixel and sampled at the 25μm pitch, resulting in a properly sampled system.

In comparison with the 256×256 microscanned system, Figure 19 shows that the oversampled system yields better contrast results as evident by the larger response at the higher frequencies. However, the oversampled system violates the constraint that the optical blur must be matched to the pixel collection area, and therefore sensitivity is not maximized and operational performance in a low signal to noise ratio environment will be degraded.

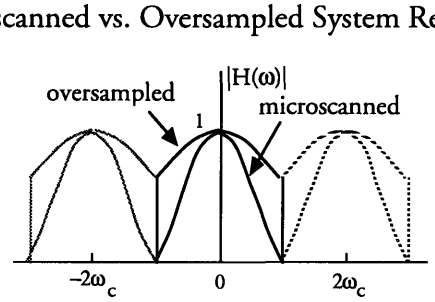

Figure 19. A comparison between the system response of the oversampled system and the microscanned system reveals that the oversampled system yields a larger response at the higher spatial frequencies.

The fourth option is obtained when a 25μm blur size (instead of 50μm) is sampled by the FPA. By sampling at the 25μm pitch with a 25μm collection area, an undersampled non-microscanned 256×256 image will result, which is basically equivalent to the 128×128 non-microscanned system but with double the spatial resolution, as shown in Figure 20. This is the *256×256 undersampled* configuration.

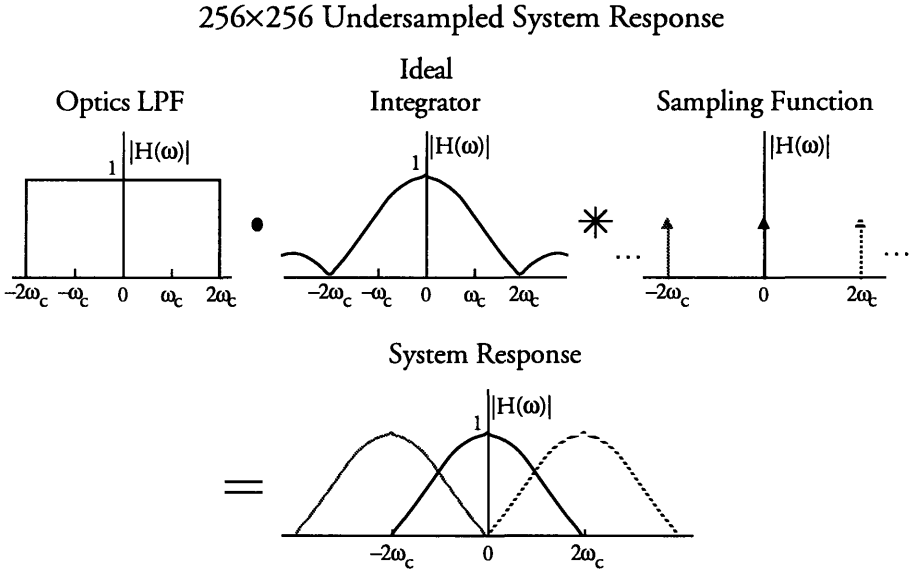

Figure 20. Spatial frequency domain system function for the one dimensional model of the 256×256 undersampled system. A 25μm blur is integrated by a 25μm pixel and sampled at the 25μm pitch, resulting in aliasing at the higher frequencies.

4. Laboratory Testing

Testing of the devices was conducted at the Raytheon Electronic Systems Division's Electro-Optics Laboratory in Tewksbury, Massachusetts from September, 1994 to March, 1995.

4.1 Optical System Setup

A generic multiband infrared optical telescope is used to enlarge and focus images on the FPA in a test dewar. The telescope optics consist of a converger optical system and a three power telescope, and is used in conjunction with a 10 inch collimator. The *f*/2 converger has an effective focal length of 1.6 inches, with a diameter of 0.8 inches. The adjustable focus *f*/2 telescope has a diameter of 2.4 inches and an effective focal length of 4.85 inches. As a system, the converger and three power telescope have an optical transmission of 81% in the mid-wave infrared band.[12] The diffraction-limited blur size of the optics at the 5μm wavelength is 25μm.

Although the optical test fixture has a focus adjustment capability, the geometry of targets is more accurately determined and the best performance obtained when the focus is set at infinity and a collimator is used to project the targets to the optics. Both the targets and the optics are placed 84 inches away from the collimator face, as shown in Figure 21. Targets are generated by placing machined aluminum plates in front of a blackbody infrared radiation source. In addition, since overhead transparency film is partially transmissive in the mid-wave IR band and toner is not, any suitable target (such as a spoke target) can be created by photocopier or laser printer.

Optical System Setup

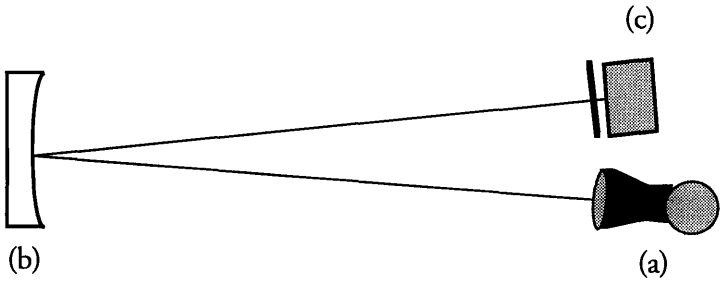

Figure 21. Optical system configuration used to test the electronic microscan device. The major components are (a) optical test fixture and test dewar, (b) collimator, and (c) blackbody radiation source.

[12] Dragon, pp. 1-4, Table 1.

4.2 Test Dewar and Support Electronics

A cryogenic test dewar houses the FPA and the electrical interconnect personality board. The dewar consists of two chambers as shown in Figure 22. The vacuum chamber contains the FPA and electrical interconnect personality board. As its name suggests, all air is evacuated from this chamber in order to prevent condensation and to enhance thermal conductive efficiency inside the dewar. A wideband-IR optical window mounted in the center of the lid can withstand extreme vacuum pressures.

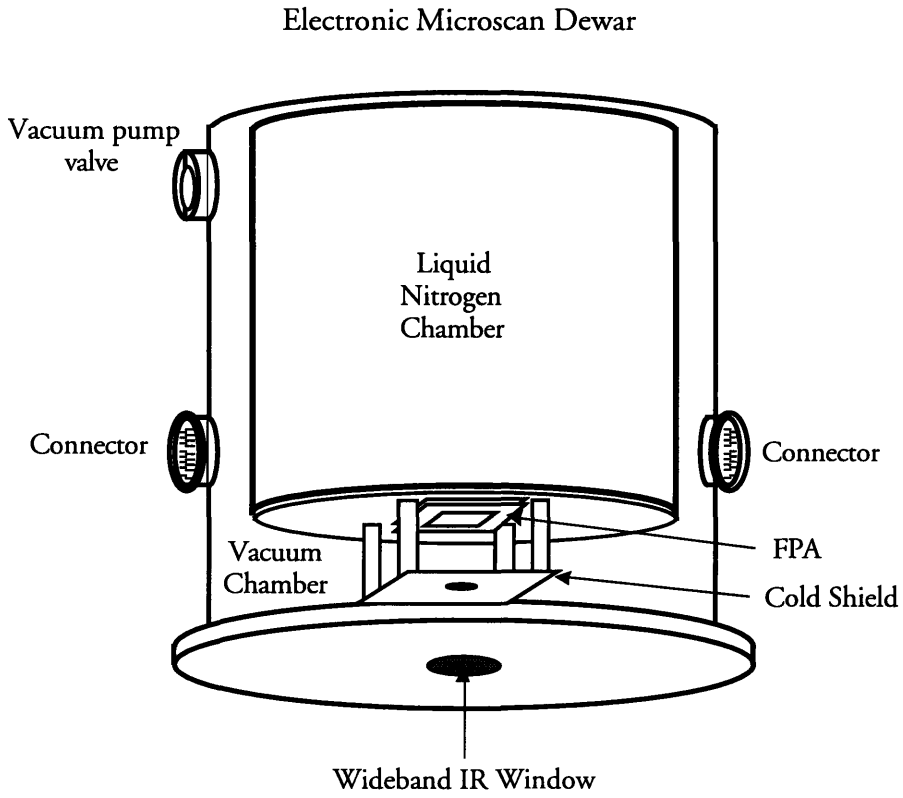

Figure 22. Diagram of the test dewar. The light enters from the bottom of the dewar and illuminates the FPA. The bottom chamber is evacuated. The top chamber is filled with liquid nitrogen and cools the array to 77°K.

The second chamber is the coolant reservoir, which is filled with liquid nitrogen. When the reservoir is full, the FPA device is cooled to the liquid nitrogen temperature of 77° Kelvin. Actual temperature of the device is confirmed by a precalibrated 2N2222A temperature diode which has been mounted on the device ceramic packaging.

Inside the dewar, located in the optical path 0.75 inches above the FPA and connected to the heat sink is a beryllium cold shield with a 0.2 inch diameter hole. The cold shield is used to prevent unwanted stray infrared radiation from being detected, and

also acts as the diffraction-limited stop for the system such that there is a 50μm blur size at the FPA. If desired, different blur sizes can be obtained by replacing the cold shield with another which has a different diameter. For some of the tests, a 0.4 inch diameter cold shield is used to obtain a 25μm blur.

There are several electrical signals and voltages which are needed for proper operation of the device. Voltages for the detector common node, the bias voltage for the active and inactive photodiodes, the current source voltage, a cascode transistor voltage and the analog and digital supplies are supplied by low-noise power supplies. Digital timing signals are also needed for the data and clock lines which are connected to each shift register and the pixel selection state machine dedicated to each column of the FPA.

An Amber Pro-View[13] imaging system provides the digital timing signals needed to drive the device. The timing of the digital signals is programmed on a personal computer, downloaded to the Pro-View system, and distributed to a digital buffer circuit card attached to the dewar via Coaxicon[14] cables. In addition to the chip's clock signals, the Pro-View is also programmed to generate the Analog-to-Digital (A/D) converter timing signals for the Pro-View's data acquisition module. The master clock frequency is adjustable so that the desired frame rate can be achieved.

The electronic microscan device requires a current source in order to drive each of the four outputs. Four custom two-stage amplifiers have been designed to supply a 100mA source for each output. The first stage of the amplifier circuit removes a DC offset from the device in order to make the output signal compatible with the ±1.5V input requirements of the Pro-View A/Ds. The second stage has a gain of 1.5 (to provide more useful dynamic range for the A/Ds), and is capable of driving the load presented by the Pro-View system and oscilloscopes. These buffer amplifiers also reside on the circuit card attached to the dewar.

4.3 Imaging System

For the laboratory portion of this thesis, the Amber Pro-View imaging system and the AE-RTAS (Amber Engineering Real-Time Application System) software provided the means for data collection, device offset and gain calibration, and data reconstruction and display. The Pro-View system is a versatile generic tool which provides flexibility for different detector configurations (including microscan operation) and requires a minimal

---

[13] Pro-View is a trademark of Amber Engineering, a division of Raytheon Company.
[14] Coaxicon is a trademark of AMP Incorporated, Harrisburg, PA USA.

amount of additional custom equipment. Programmable clock rates are standard, with video frame updating synchronized to either the device or the master video output signal.

Whereas the Pro-View system allows for convenient data capture, its data analysis tools are limited to region-of-interest (ROI) extraction, histogram thresholding, and simple single frame manipulations. Although a programmable language environment exists to develop more robust image manipulation routines, the electronic microscan data was exported so that Matlab and Excel (technical spreadsheet) analysis could be performed offline.

4.4 Microscanning Test Plan

The primary task is to verify that microscanning can be performed by the detector ROE. Signal to Noise ratio (SNR) performance evaluations under different configurations are to be left for a future effort. Consequently, a maximum SNR is desired during each of the tests. To that end, the blackbody radiation source is cranked up to its maximum temperature (resulting in a ΔTemperature of 30°C) when presenting targets to the FPA.

Since the MTF is of primary importance when evaluating the electronic microscan device, standard bar targets are used to present binary signals with varying spatial frequencies, and the contrast is determined using (3). The MTF curve of the device is estimated from the data points collected at the minimum and maximum observed contrast. This method is used for each of the system configurations.

Pixel collection area plays a major role in determining the MTF of the system. A multiple ramp spread method will be used to estimate the extent of the pixel's sensitive region. Assuming nonuniformities are corrected during the calibration procedure by the ProView system and a fairly homogeneous collection function exists across the array, the pixel response to a knife-edge input can be estimated by imaging a slightly slanted horizontal line. The line is assumed to cross the center of the row at column with the largest response. By determining the line crossings over several rows, one can determine the distance between the line and the center of the pixel for all pixels, and build a collection area profile, which must then be deconvolved with the line spread function (sinc function) to obtain the actual collection function. This procedure is shown in Figure 23.

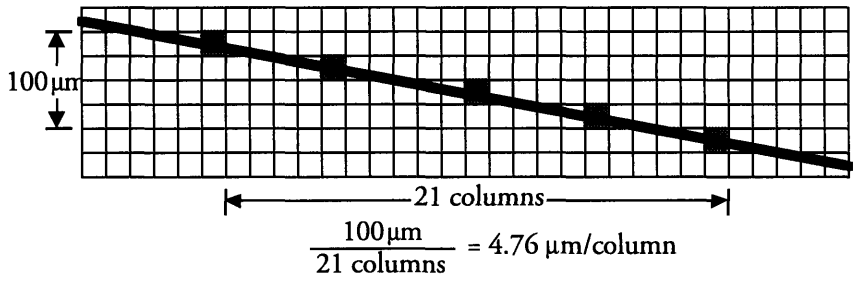

(a) Image a skewed horizontal line and select the pixel in each row with the peak response (which should correspond to where the line is centered in the pixel). Calculate the column unit distance by dividing the distance covered by the peaks by the number of columns between peaks.

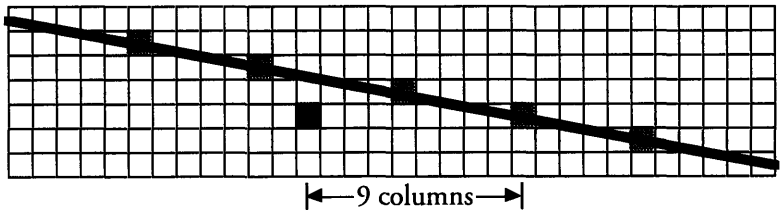

(b) Assuming an almost horizontal line, the vertical distance between any pixel and the line is determined by multiplying the column unit distance by the number of columns between the peak and pixel. The black pixel is 42.9µm below the line.

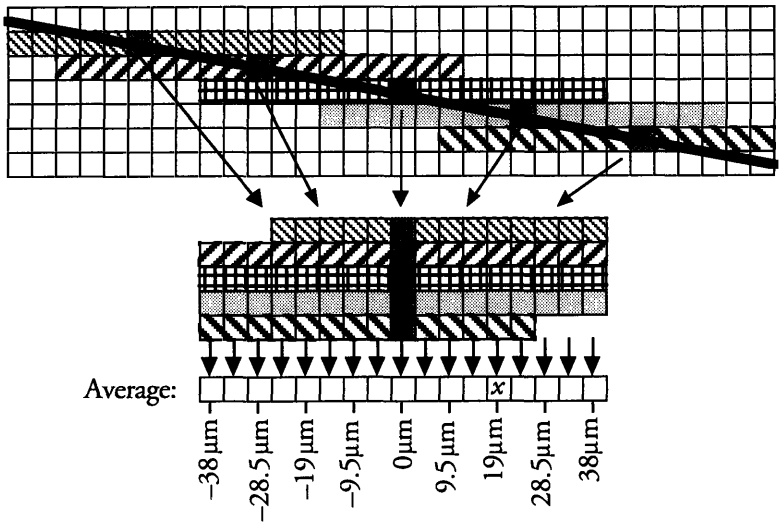

(c) An estimate of the linear collection area is obtained by aligning each of the peak pixels and averaging the column responses. For example, x is the average response to a line 19µm below the pixel. The results must be deconvolved with the sinc line spread function.

Figure 23. Ramp spread procedure used to estimate the linear collection area of a pixel by imaging a slanted line.

Microscanning also has a dramatic impact on the reduction of nonisoplanatic effects. Although the minimum MTF is measured while examining the bar targets, there is no easy method for quantifying how often these effects occur. As discussed by Bradley, Baddiley, and Dennis,[15] the worst of the nonisoplanatic effects in a typical FPA occur only for a fraction of the possible input signal phases, and both the quantity of possible phases which contain these effects and the magnitude of the effects are reduced by microscanning. Consequently, a subjective comparison of a slowly moving bar target shall be made for each of the operational modes.

Finally, a spoke target will be imaged in each configuration. Assuming that portions of the spoke target reach a spatial frequency which exceeds the Nyquist frequency for the system, the aliasing effects should be evident. This method provides another qualitative means of system aliasing analysis. The spoke target was taken from Goodman[16] and is shown in Figure 24.

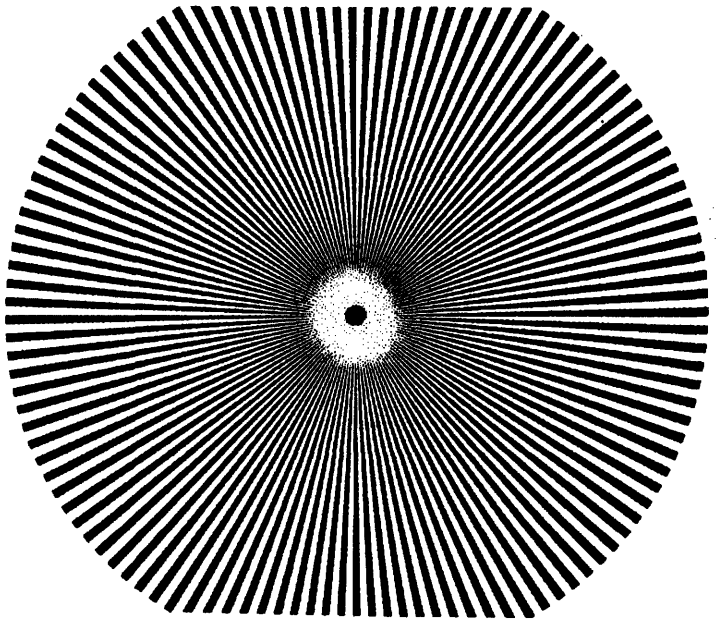

Figure 24. Imaging this spoke target is a convenient qualitative way to observe aliasing (from Goodman, p. 126).

[15] Bradley et al., 1987, p. 39.
[16] Goodman p. 126.

4.5 Laboratory Results

Two different devices were evaluated for this thesis. Each had its own set of unique characteristics which have been accounted for in the data analysis. Device #1 was used for most of the preliminary electronic and imaging system validation, and tended to provide unreliable data since it developed an excessive number of unresponsive or unusable pixels. Device #2 had a much more consistent response, but only one quarter of the array was usable in the microscanning mode. However, each of the tests was performed and the data collected from the best region possible. Where practical, multiple measurements were taken and averaged to reduce the variance in the data.

The results of the bar target MTF curve generation are shown in Figure 25 and Figure 26. Although the data points do not exactly match the predicted MTF curve, the maximum (solid) microscan and non-microscan curves are similar to each other (curve fitting is difficult with only five data points). Taking into consideration the minimum (dotted) MTF curves, nonisoplanatic effects are reduced in the microscan system, as indicated by the reduced disparity between the dotted and solid lines. This data set was taken from device #1.

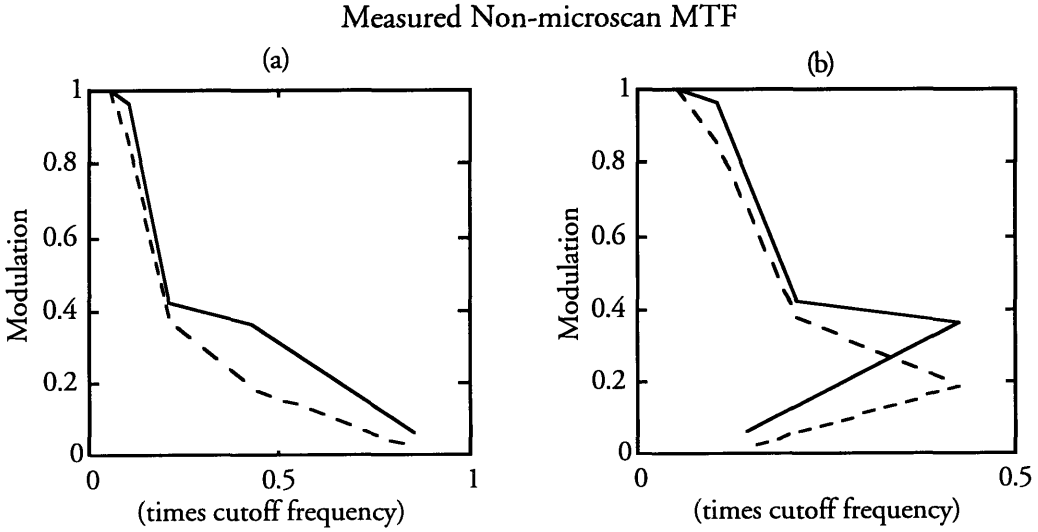

Figure 25. Measured MTF from device #1 for non-microscan system (a) as a function of input frequency, and (b) as a function of output frequency.

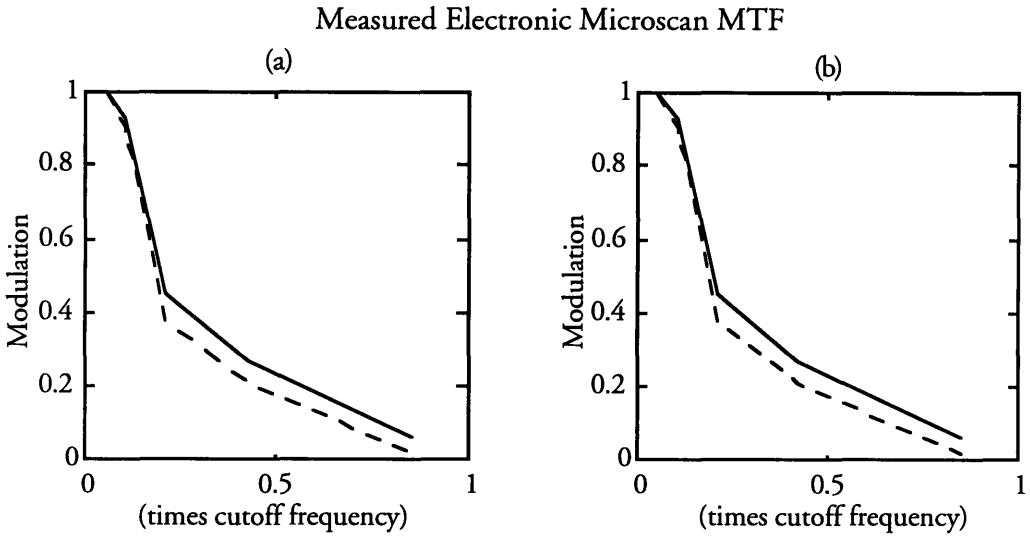

Figure 26. Measured MTF from device #1 for microscan system (a) as a function of input frequency, and (b) as a function of output frequency.

The most quantifiable results were obtained from the ramp spread function analysis. Figure 27 shows the linear response seen from device #2 in the microscan and non-microscan mode. After deconvolving the response with a 25μm sinc function, it appears that the responsive region increased from approximately 25μm to 40μm as predicted. Analysis of device #1 yielded similar but noisier results. The predicted linear collection area profiles are shown in Figure 28, and are the result of convolving the 50μm Airy disk with a 25μm tapered boxcar and a 40μm Gaussian curve. The difference between the predicted results and the actual laboratory results is due to the fact that the actual collection area is not Gaussian as the model suggests.

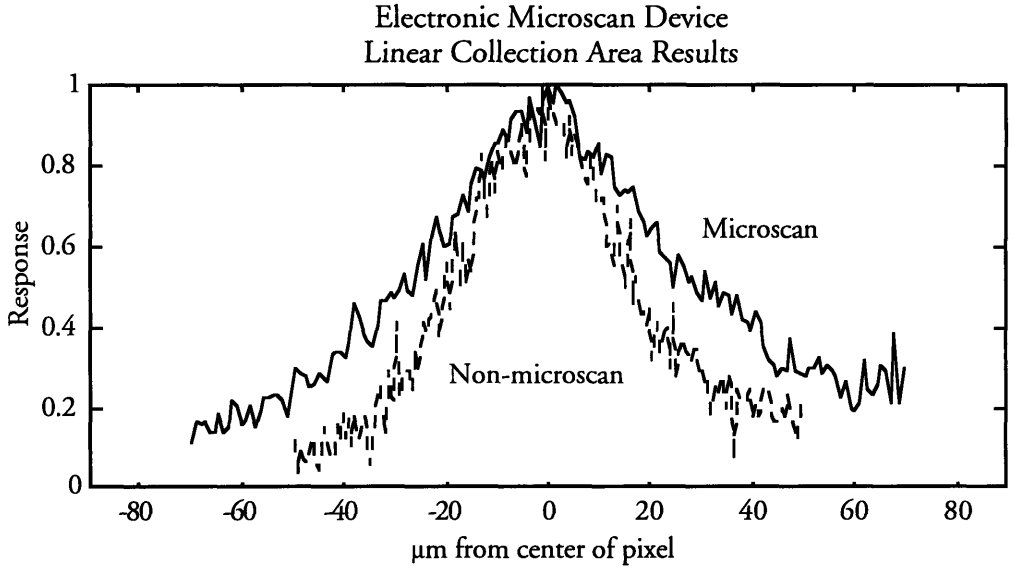

Figure 27. Linear collection area profile of typical pixel on electronic microscan device #2. After deconvolving the profile with a 25μm sinc function, based on the 50% response point the non-microscanned pixel diameter was found to be about 25μm and the microscanned pixel diameter was approximately 40μm.

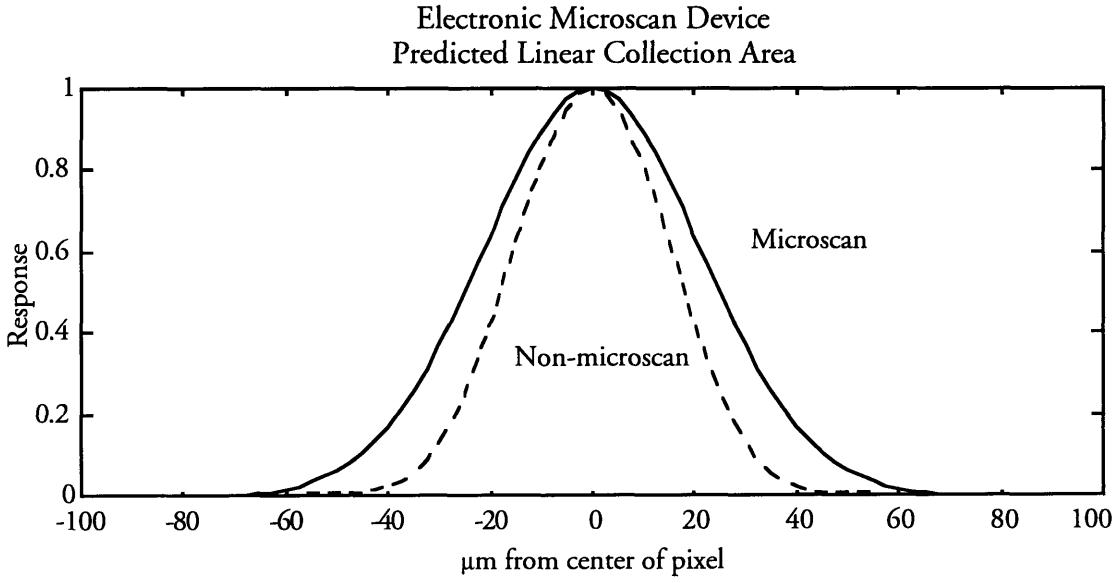

Figure 28. Predicted linear collection area profile of pixel on the electronic microscan device. The non-microscan model was obtained by convolving a 50μm Airy disk with a 25μm tapered boxcar function. The microscan model was obtained by convolving a 50μm Airy disk with a 40μm Gaussian function.

During the tests, the smallest distinguishable bar targets were slowly moved across the image in order to visualize the nonisoplanatic effects. During non-microscan operation in either the 128×128 or 256×256 mode, the bars appeared and disappeared as the scene panned. When microscanning was enabled, the bars traversed the image much more smoothly and appeared more natural, confirming the predicted reduction in phase-dependent effects.

A transparency of Goodman's spoke target was imaged in each of the four modes. Although the spatial frequency of the target exceeded the Nyquist frequency for all of the systems, it was difficult to compare the various 256×256 images due to the poor contrast of the target and the noisiness within the image. A careful examination of each spoke image reveals results consistent with the predictions. Figure 29 contains pictures of the spoke targets captured in each mode by a Mitsubishi P51U video printer, which exacerbated the problem of presenting concise results by quantizing the original image into 14 discrete levels of gray.

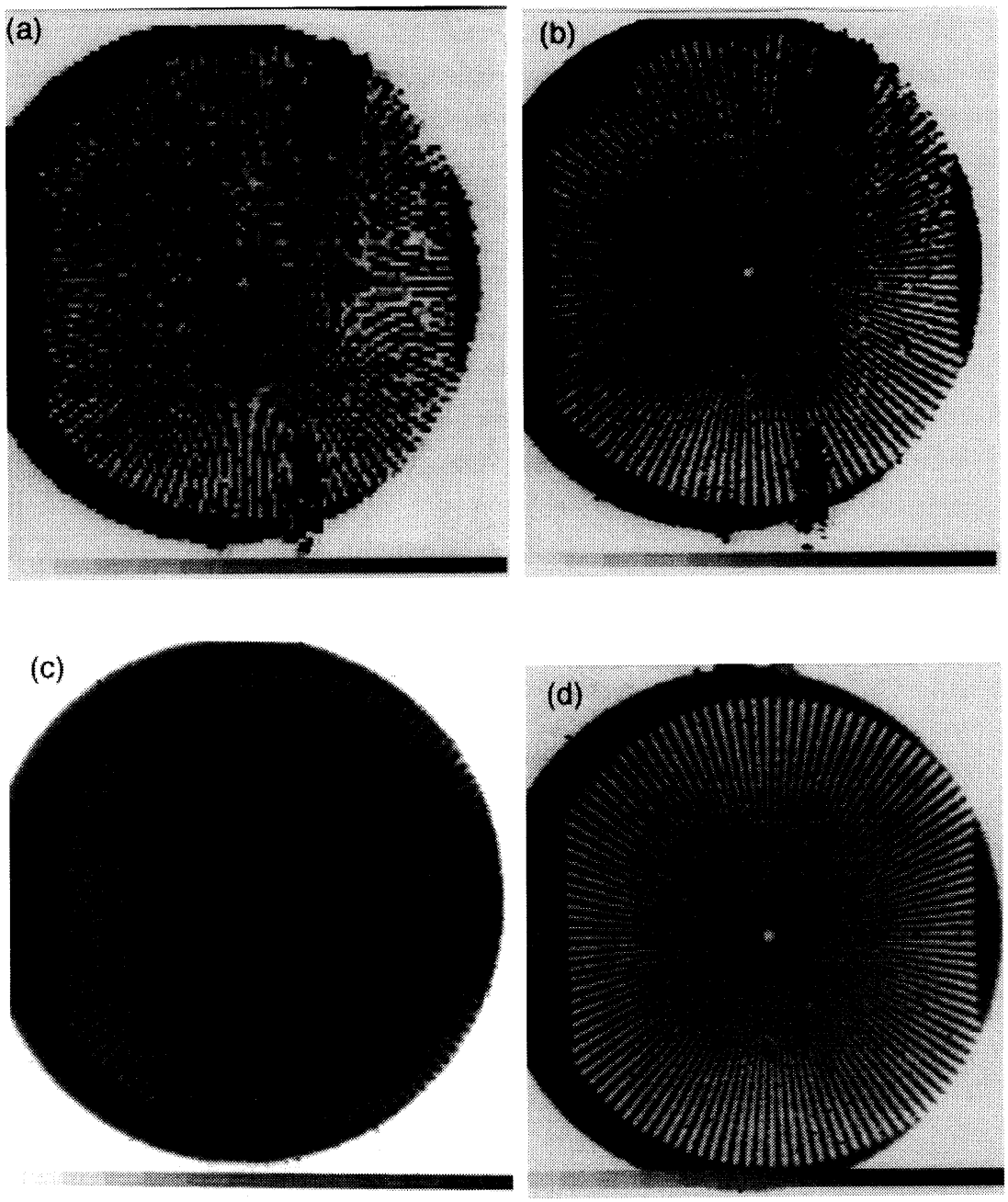

Figure 29. Spoke Targets taken in the following configurations: (a) 128×128 non-microscan, (b) 256×256 microscan, (c) 256×256 undersampled, (d) 256×256 oversampled.

5. Discussion and Conclusion

5.1 System Considerations

This thesis showed that overlapping pixel collection areas can be obtained through this electronic microscanning method. Assuming the requirement that the optical blur size is matched to the pixel collection area, microscanning provides the best performance for a non-aliasing system. Electronic microscanning is convenient because additional circuitry, filters and motors are not needed to achieve good results. Since the collection area is directly dependent upon the diffusion length of the material used, the integration function can be tailored without a change to the ROE design.

Obviously, the MTF performance of the microscanned 256×256 system is better than the 128×128 system, if only for the increase in the sampling frequency by a factor of two in each direction. Consequently, the discussion remains which of the 256×256 modes best match the objectives. The electronic microscan mode satisfies the need to have an overlapping sampling area, with the virtual elimination of aliasing.

As shown in section 3.2, the best spatial frequency response is obtained by the ideal 256×256 oversampled system, which will satisfy the Nyquist criteria and provide better response at the higher frequencies than the microscanned system. This could be most beneficial for automatic target recognition (ATR) algorithms which require maximum accuracy and distingushability, especially at the higher frequencies. However, the oversampled system does not maximize system sensitivity since the pixel collection area is not matched to the blur size. Hence, a tradeoff exists which must be considered carefully. Perhaps the tradeoff conflict can be mediated by utilizing electronic microscanning while in low signal to noise ratio conditions (taking advantage of the added sensitivity due to the matched blur size), and switching to the reduced collection area for automatic target recognition algorithm use (with improved response at higher frequencies).

Another item to consider is that the spatial cutoff frequency has been limited by the 50μm blur size in the preceding two configurations discussed. In a sense, the electronic microscan array is a derated 256×256 25μm array. By utilizing a 25μm blur size in the undersampled 256×256 system, higher frequencies can be sensed but they would be aliased. The MTF of the undersampled system matches the curve of the 256×256 oversampled system for the nonaliased lower half of the frequencies, which yielded the best contrast results. The upper half of the frequencies are detectable but aliased. With the 256×256 undersampled system, the best MTF contrast results and the higher spatial

resolution are obtained at the expense of aliasing. Thus, the tradeoff between cutoff frequency, response, and aliasing must be considered.

5.2 Suggestions for Further Research

Electronic microscanning takes advantage of the characteristics of a floating photodiode to create overlapping pixel collection areas in a focal plane array. Preliminary investigation into the impact of the electronic microscan configuration on system noise is not encouraging. Unfortunately, floating intrinsic photodiodes may create excessive leakage current, and contribute to 1/f noise, reducing the useful dynamic range of the device. Further research by device physicists into the reduction of this leakage current (i.e. by using extrinsic semiconductor devices) might make electronic microscanning a more useful alternative. Other options might include finding a way to redirect the leakage current without affecting the carrier diffusion by shunting the leakage in a manner similar to anti-blooming strips.

Since the pixel collection area was not uniform and completely overlapping, the electronic microscan device is not the ideal FPA oversampler. As device geometries shrink further, alternative configurations (such as a 3×3 microscan) might fill in the gaps and more completely sample the scene.

The diffusion length of the material is a fundamental component of the electronic microscan performance. Additional research into the use of different materials (to achieve more complete overlapping samples) might be useful.

6. Bibliography

K. Awamoto, Y. Ito, H. Ishizaki, and Y. Yoshida, Resolution Improvement for HgCdTe IRCCD," SPIE Vol. 1685, *Infrared Detectors and Focal Plane Arrays II*, 1992.

K.J. Barnard, "Nonmechanical Microscanning Using Optical Space-Fed Phased Arrays," (Final Report for Summer Faculty Research Program, Wright Laboratory), Memphis State University, 1993.

M. Born and E. Wolf, *Principles of Optics*, Pergamon Press, Oxford/New York, 1980.

D.J. Bradley, C.J. Baddiley, and P.N.J. Dennis, "The Modulation Transfer Function of Focal Plane Array Systems," SPIE Vol. 807, *Passive Infrared Systems and Technology*, 1987.

D.J. Bradley, and P.N.J. Dennis, "Sampling Effects in CdHgTe Focal Plane Arrays," SPIE Vol. 590, *Infrared Technology and Applications*, 1985.

R.J. Dann, S.R. Carpenter, C. Seamer, P.N.J. Dennis, and D.J. Bradley, "Sampling Effects in CdHgTe Focal Plane Arrays - Practical Results," SPIE Vol. 685, *Infrared Technology XII*, 1986.

M.S. Dragon, "IR Initiative Optical Design and Analysis (7607:91:163)," Raytheon Company Internal Memo, 1991.

Goodman, *Introduction to Fourier Optics,* McGraw-Hill, New York, 1968.

G.C. Holst, "Sampling Effects in Imaging Systems," Spectral Reflections Technote 94-03, 1994.

L. Lambert, "Optical Scanning Techniques (93R-195)" Raytheon Company Internal Memo, 1993.

A.H. Lettington, Q.H. Hong, J. Macdonald, A. Marshall, K. Murphy, and P.P. Donohue, "Measurement of the MTF and MRTD for Focal Plane Arrays," SPIE Vol. 1969, *Infrared Imaging Systems: Design, Analysis, Modeling, and Testing IV*, 1993.

R. Lenz and U. Lenz, "Calibration of a Color CCD camera with 3000×2300 Picture Elements," SPIE Vol. 1395, *Close-Range Photogrammetry Meets Machine Vision*, 1990.

S. Liberman, "Modeling of Cross-Talk in Backside Illuminated FPA's," Raytheon Company Internal Memo, 1994.

J.S. Lim, *Two-Dimensional Signal and Image Processing*, Prentice Hall, 1990.

S.C. Luongo, Personal Interview, March 4, 1995.

P.F. McManamon, E.A. Watson, T.A. Dorschner, and L.J. Barnes, "Applications Look at the Use of Liquid Crystal Writable Gratings for Steering Passive Radiation," Optical Engineering Vol. 32-11, 1993.

P.F. McManamon, E.A. Watson, T.A. Dorschner, and L.J. Barnes, "Nonmechanical Beam Steering for Active and Passive Sensors," SPIE Vol. 1969, *Infrared Imaging Systems: Design, Analysis, Modeling, and Testing IV*, 1993.

B.A. Muse, A.E. Absi, F.P. Blommel, and E.A. Watson, "Comparison of Staring Versus Microscan Recognition Range Performance," Wright Laboratory, Avionics Directorate, Electro-Optics Branch, Wright-Patterson AFB, OH, 1994.

R.A. Muse, "Spatial Sampling of Staring Infrared Focal Plane Arrays," ELE 573, Electro-Optical Devices and Systems, University of Dayton, 1992.

A.V. Oppenheim, and R.W. Shafer, *Discrete-Time Signal Processing*, Prentice Hall, 1989.

I.J. Spiro, and M. Schlessinger, *Infrared Technology Fundamentals*, Marcel Dekker, Inc., New York, 1989.

E.G. Stewart, *Fourier Optics: An Introduction*, John Wiley & Sons, New York, 1983.

E.A. Watson, R.A. Muse, and F.P. Blommel, "Aliasing and Blurring in Microscanned Imagery," SPIE Vol. 1689, *Infrared Imaging Systems*, 1992.

J. Wey, "Microscan Analysis," Raytheon Company Internal Memo, 1994.

R.L. Wildey, "The Nyquist Criterion in CCD Photometry for Surface Brightness," Publications of the Astronomical Society of the Pacific, Vol. 104, April, 1992.

W. Wittenstein, J.C. Fontanella, A.R. Newbery, and J. Baars, "The Definition of the OTF and the Measurement of aliasing for Sampled Imaging Systems," Optica Acta, Vol. 29-1, 1982.

Appendix 1 - Matlab Simulation Files

fig8.m - generates MTF curve for non-microscanned system:

```
% This is the 100% fill factor MTF generator for 50µm simulated non-
        µs system
% This file calculates MTF of
% 50µm sampling interval of 50µm blur
% with ideal boxcar collection area
%

clear
clg
echo on

% Create index array
index=[1:1:1100];

% predefine the maximum and minimum vectors which will be plotted
        later...
% we are calculating mtf in 0.05*cutoff intervals up to 2*cutoff so
        there will be
% 40 entries in the table
maxmtf=zeros(2,40);
minmtf=zeros(2,40);

% Define averaging function for 20 points per sample, based on an
        ideal boxcar (50µm collection area)
% 20 points = 50 µm
avg=ones(20,1)/20;

for loop=1:39;
PctNyq = loop/20
% Create cosine wave (0≤x≤1)
% there are 20 phase shifted versions of the sine wave interlaced...
x=0.5+cos(pi*index*PctNyq/20)/2; % 0<x<1 version

blurincr50=5.5/20; % want bessel of |-2.75 to 2.75| for blur size,
        50µm blur (from blur=0.1)
blur50=(2*bessel(1,abs(-
        19.5*blurincr50:blurincr50:19.5*blurincr50))./abs(-
        19.5*blurincr50:blurincr50:19.5*blurincr50)).^2;

% First, convolve the input signal with the blurs.
xblur50=conv(blur50,x);

% convolve the averaging function with the input to create 20
        versions of the input
% each with different phase (πn/10)
% xavg is 1000+20-1 points long, so the first valid point is xavg[20]
xavg=conv(avg,xblur50); % 50µm normal and microscanned data
```

```
% Separate the averaged functions into individual phase-shifted
       sampled functions:
% the first valid sample is number 60
% sample every 20 points = 50 µm, every 10 points = 25 µm
xsamp=zeros(40,20);

for a = 1:40,
    for b = 1:20,
       xsamp(a,b)=xavg(b+59+a*20); %128x128 non-microscanned
    end
end

% create a vector of one of the phases,
% and compute FFT to determine frequency
xrep=(xsamp(1:40,1));
XREP = abs(fft(xrep));

% XREP goes from 0 to 2π, we are only interested in which bin between
       0 and π is positive
% i contains the index of the peak. (ignore DC term)
[y,i]=max(XREP(2:21));

% find the peak value of x at each phase (only search over one
       percieved period)
% and determine the contrast (maxpeak - minpeak) at each phase to get
       MTF
xsampmax=max(xsamp(1:max(min(40,round((40/i)+.5)),2),1:20));
xsampmin=min(xsamp(1:max(min(40,round((40/i)+.5)),2),1:20));
xmtf=(xsampmax-xsampmin)./(xsampmax+xsampmin);
xmax=max(xmtf);
xmin=min(xmtf);

maxmtf(1,PctNyq*20)=i; %save perceived frequency index, accounting
       for ignoring DC
maxmtf(2,PctNyq*20)=xmax;
minmtf(1,PctNyq*20)=i; %save perceived frequency index, accounting
       for ignoring DC
minmtf(2,PctNyq*20)=xmin;

end

subplot (121);
axis ([0,1.1,0,1]);
plot (((1:1:39)./40),maxmtf(2,1:39),'-
       ',((1:1:39)./40),minmtf(2,1:39),'--')
title ('(a)');

subplot (122);
axis ([0,0.55,0,1]);
plot ((maxmtf(1,1:39)./40),maxmtf(2,1:39),'-
       ',(minmtf(1,1:39)./40),minmtf(2,1:39),'--')
```

```
title ('(b)');
subplot (111);
title ('Non-Microscanned MTF');
```

fig10.m - generates MTF curve for 2× microscanned system:

```
% This is the 100% fill factor MTF generator for 50µm simulated. µs
        system
%
% microscanned 256x256 system  (50µm blur, 25µm pitch, 50µm pixel)
%

clear
clg
echo on

% Create index array
index=[1:1:1100];

% predefine the maximum and minimum vectors which will be plotted
        later...
% we are calculating mtf in 0.05*Nyquist intervals up to 2*Nyquist so
        there will be
% 40 entries in the table
maxmtf=zeros(2,40);
minmtf=zeros(2,40);
maxusmtf=zeros(2,40);
minusmtf=zeros(2,40);

% Define averaging function for 20 points per sample, based on an
        ideal boxcar (50µm collection area)
% 20 points = 50 µm
avg=ones(20,1)/20;

for loop=1:39;
PctNyq = loop/20
% Create cosine wave (0≤x≤1)
% there are 20 phase shifted versions of the sine wave interlaced...
x=0.5+cos(pi*index*PctNyq/20)/2; % 0<x<1 version

blurincr50=5.5/20; % want bessel of |-2.75 to 2.75| for blur size,
        50µm blur
blur50=(2*bessel(1,abs(-
        19.5*blurincr50:blurincr50:19.5*blurincr50))./abs(-
        19.5*blurincr50:blurincr50:19.5*blurincr50)).^2;

% First, convolve the input signal with the blurs.
xblur50=conv(blur50,x);

% convolve the averaging function with the input to create 20
        versions of the input
% each with different phase (πn/10)
```

```
% xavg is 1000+20-1 points long, so the first valid point is xavg[20]
xavg=conv(avg,xblur50); % 50µm normal and microscanned data

% Separate the averaged functions into individual phase-shifted
       sampled functions:
% the first valid sample is number 60
% sample every 20 points = 50 µm, every 10 points = 25 µm
xuscan=zeros(80,20);
for a = 1:40,
    for b = 1:20,
       xuscan(2*a-1,b)=xavg(b+59+a*20); % 256x256 microscanned
       xuscan(2*a,b)=xavg(b+59+a*20+10);
    end
end

% create a vector of one of the phases,
% and compute FFT to determine frequency
xusrep=(xuscan(1:80,1)); % 80-point FFT for microscanned...index is
       2X XREP's index
XUSREP = abs(fft(xusrep));

% XREP goes from 0 to 2π, we are only interested in which bin between
       0 and π is positive
% i contains the index of the peak. (ignore DC term)
[usy,usi]=max(XUSREP(2:41));

% find the peak value of x at each phase (only search over one
       percieved period)
% and determine the contrast (maxpeak - minpeak) at each phase to get
       MTF

xuscanmax=max(xuscan(1:max(min(80,round((80/usi)+.5)),2),1:20));
xuscanmin=min(xuscan(1:max(min(80,round((80/usi)+.5)),2),1:20));
xusmtf=(xuscanmax-xuscanmin)./(xuscanmax+xuscanmin);
xusmax=max(xusmtf);
xusmin=min(xusmtf);

maxusmtf(1,PctNyq*20)=usi; %save perceived frequency index,
       accounting for ignoring DC
maxusmtf(2,PctNyq*20)=xusmax;
minusmtf(1,PctNyq*20)=usi; %save perceived frequency index,
       accounting for ignoring DC
minusmtf(2,PctNyq*20)=xusmin;

end

subplot (121);
axis ([0,1.1,0,1]);
plot (((1:1:39)./40),maxusmtf(2,1:39),'-
       ',((1:1:39)./40),minusmtf(2,1:39),'--');
title ('(a)');
```

```
subplot (122);
axis ([0,1.1,0,1]);
plot ((maxusmtf(1,1:39)./40),maxusmtf(2,1:39),'-
       ',(minusmtf(1,1:39)./40),minusmtf(2,1:39),'--')
title ('(b)');

subplot (111);
title ('Microscanned MTF')
```

fig15.m - generates MTF plot of electronic microscan device:

```
% This is the Gaussian fill factor MTF generator for 40μm diffusion
       length simulated μscan system
%

clear
clg
echo on

% Create index array
index=[1:1:1100];

% predefine the maximum and minimum vectors which will be plotted
       later...
% we are calculating mtf in 0.05*Nyquist intervals up to 2*Nyquist so
       there will be
% 40 entries in the table
maxusmtf=zeros(2,40);
minusmtf=zeros(2,40);

% Define averaging function for 20 points per sample, based on a
       gaussian (50μm collection area)
% 20 points = 50 μm
avg=exp(-1*abs((-0.95:.1:0.95).^2))./14.94; % Normalize so that
       integral=1

for loop=1:39;
PctNyq = loop/20
% Create cosine wave (0≤x≤1)
% there are 20 phase shifted versions of the sine wave interlaced...
x=0.5+cos(pi*index*PctNyq/20)/2; % 0<x<1 version

blurincr50=5.5/20; % want bessel of |-2.75 to 2.75| for blur size,
       50μm blur
blur50=(2*bessel(1,abs(-
       19.5*blurincr50:blurincr50:19.5*blurincr50))./abs(-
       19.5*blurincr50:blurincr50:19.5*blurincr50)).^2;

% First, convolve the input signal with the blurs.
xblur50=conv(blur50,x);
```

```
% convolve the averaging function with the input to create 20
       versions of the input
% each with different phase (πn/10)
% xavg is 1000+20-1 points long, so the first valid point is xavg[20]
xavg=conv(avg,xblur50); % 50μm normal and microscanned data

% Separate the averaged functions into individual phase-shifted
       sampled functions:
% the first valid sample is number 60
% sample every 20 points = 50 μm, every 10 points = 25 μm
xuscan=zeros(80,20);
for a = 1:40,
    for b = 1:20,
        xuscan(2*a-1,b)=xavg(b+59+a*20); % 256x256 microscanned
        xuscan(2*a,b)=xavg(b+59+a*20+10);
    end
end

% create a vector of one of the phases,
% and compute FFT to determine frequency
xusrep=(xuscan(1:80,1)); % 80-point FFT for microscanned...index is
       2X XREP's index
XUSREP = abs(fft(xusrep));

% XUSREP goes from 0 to 2π, we are only interested in which bin
       between 0 and π is positive
% i contains the index of the peak. (ignore DC term)
[usy,usi]=max(XUSREP(2:41));

% find the peak value of x at each phase (only search over one
       percieved period)
% and determine the contrast (maxpeak - minpeak) at each phase to get
       MTF
xuscanmax=max(xuscan(1:max(min(80,round((80/usi)+.5)),2),1:20));
xuscanmin=min(xuscan(1:max(min(80,round((80/usi)+.5)),2),1:20));
xusmtf=(xuscanmax-xuscanmin)./(xuscanmax+xuscanmin);
xusmax=max(xusmtf);
xusmin=min(xusmtf);

maxusmtf(1,PctNyq*20)=usi+1; %save perceived frequency index,
       accounting for ignoring DC
maxusmtf(2,PctNyq*20)=xusmax;
minusmtf(1,PctNyq*20)=usi+1; %save perceived frequency index,
       accounting for ignoring DC
minusmtf(2,PctNyq*20)=xusmin;

end

subplot (121);
axis ([0,1.1,0,1]);
```

```
plot (((1:1:39)./40),maxusmtf(2,1:39),'-
        ',((1:1:39)./40),minusmtf(2,1:39),'--');
title ('(a)');

subplot (122);
axis ([0,1.1,0,1]);
plot ((maxusmtf(1,1:39)./40),maxusmtf(2,1:39),'-
        ',(minusmtf(1,1:39)./40),minusmtf(2,1:39),'--')
title ('(b)');

subplot (111);
title ('Electronic Microscan MTF')
```

fig26.m - generates predicted linear response for microscan and non-microscan configuration

```
% For all plots: 20 samples = 50µm

% 50µm Airy disk
blurincr50=5.5/20; % want bessel of |-2.75 to 2.75| for blur size,
        50µm blur
blur50=(2*bessel(1,abs(-
        19.5*blurincr50:blurincr50:19.5*blurincr50))./abs(-
        19.5*blurincr50:blurincr50:19.5*blurincr50)).^2;


% Gaussian function for 40µm collection area
gauss40=exp(-1*abs((-1.95:.1:1.95).^2));

% Tapered 25µm Boxcar
box=zeros(1,40);
box(16:25)=ones(1,10)./11;
box(15)=2/33;
box(26)=2/33;
box(14)=1/33;
box(27)=1/33;

% Non-microscan predicted line spread response:
nouspred=conv(box,blur50);
% Microscan predicted line spread response:
uspred=conv(gauss40,blur50);

%Normalize them both
nouspred=nouspred./(max(nouspred));
uspred=uspred./(max(uspred));

plot ((-97.5:2.5:97.5),uspred,'-',(-97.5:2.5:97.5),nouspred,'--');
```

Appendix 2 - Data

Image Data

Image of non-microscanned line used for linear collection area analysis:

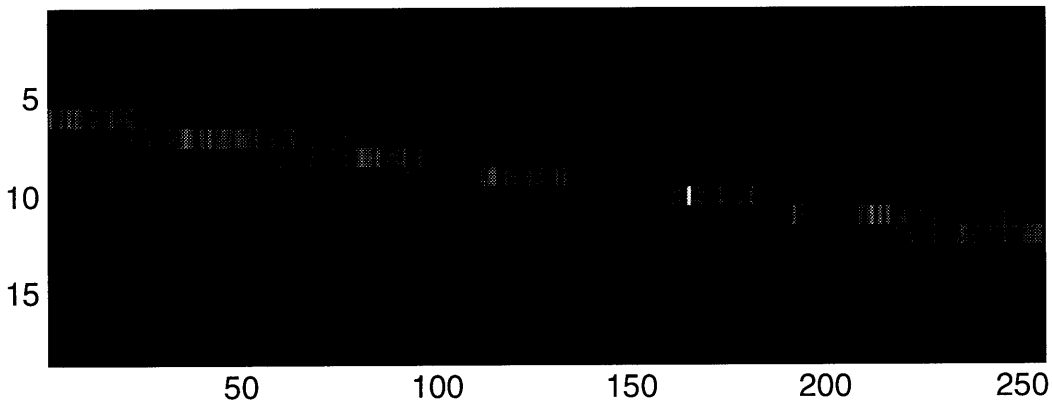

Image of microscanned line used for linear collection area analysis:

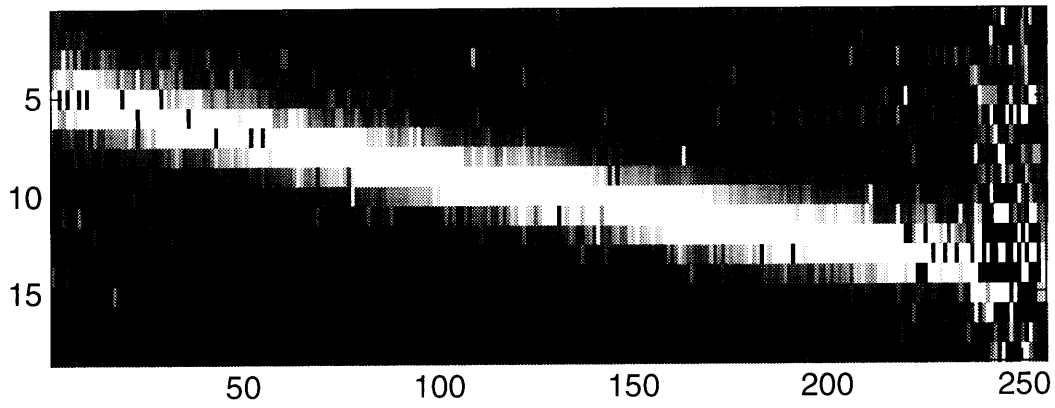

MTF data of non-microscanned system

Output Freq.				Normalized:	
(% Cutoff)	Target	Max MTF	Min MTF	Max MTF	Min MTF
0.053	A	200.000	200.000	1.000	1.000
0.107	B	192.000	170.000	0.960	0.850
0.214	C	84.000	75.000	0.420	0.375
0.428	D	72.000	37.000	0.360	0.185
0.145	E	13.000	4.000	0.065	0.020

Non-Microscanned Target Responses

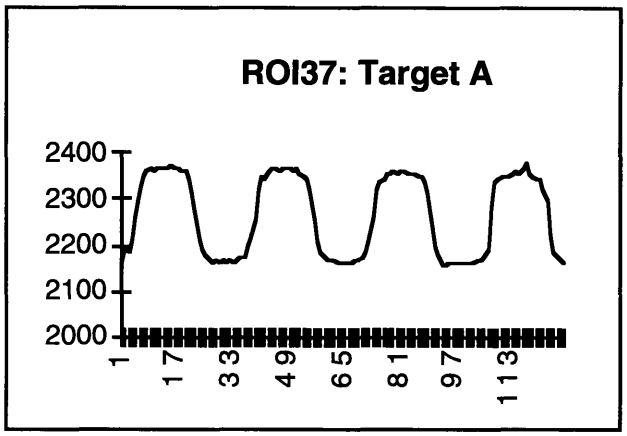

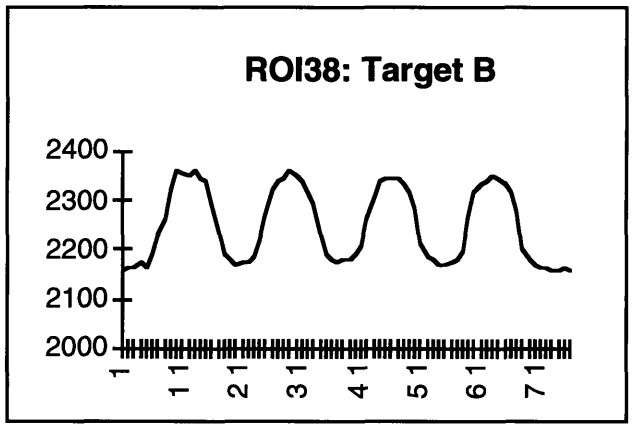

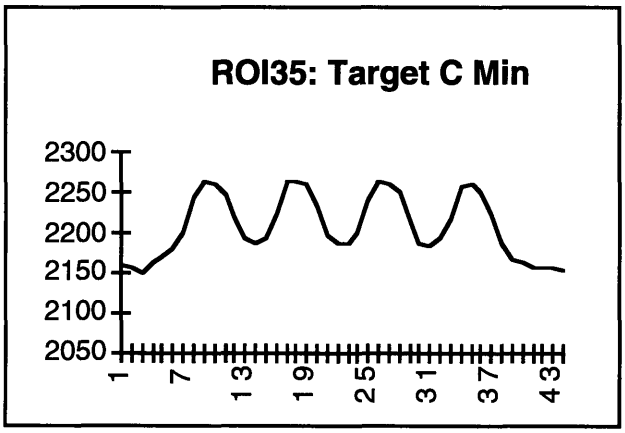

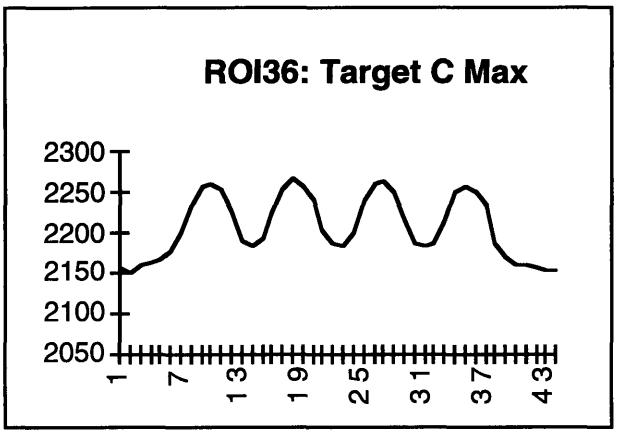
ROI36: Target C Max
2300
2250
2200
2150
2100
2050
1
7
13
19
25
31
37
43

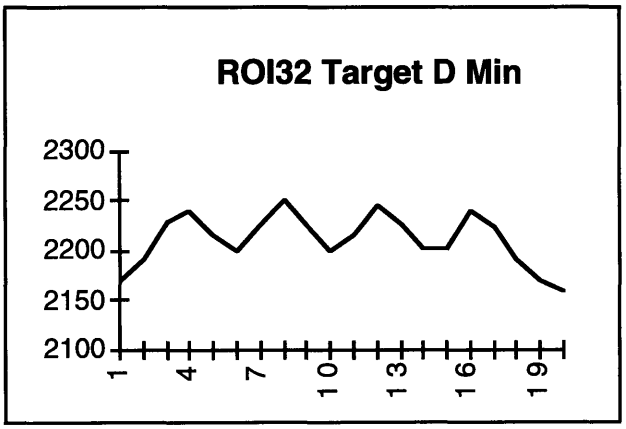
ROI32 Target D Min
2300
2250
2200
2150
2100
1
4
7
10
13
16
19

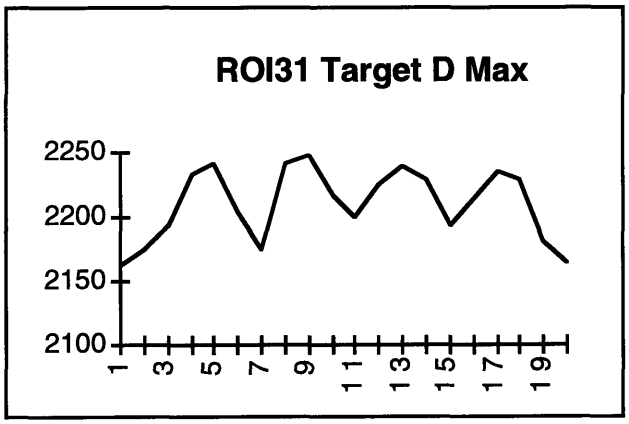
ROI31 Target D Max
2250
2200
2150
2100
1
3
5
7
9
11
13
15
17
19

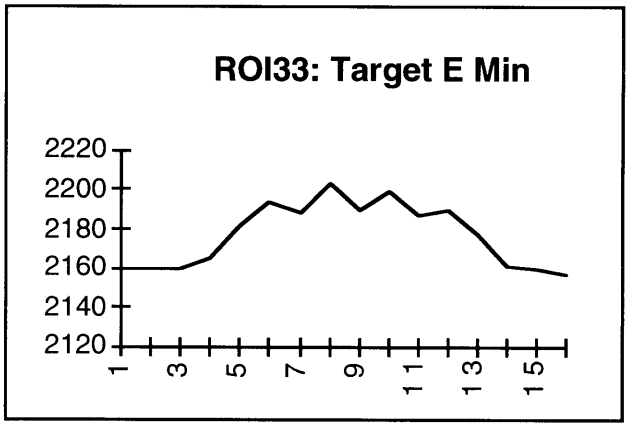

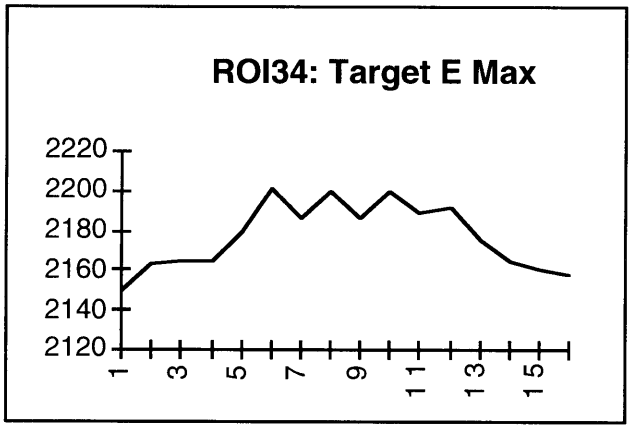

MTF data of microscanned system

				Normalized:	
%Cutoff	Target	Max MTF	Min MTF	Max MTF	Min MTF
0.053	A	199.000	199.000	1.000	1.000
0.107	B	185.000	180.000	0.930	0.905
0.214	C	90.000	75.000	0.452	0.377
0.428	D	53.000	42.000	0.266	0.211
0.855	E	12.000	3.000	0.060	0.015

Microscanned Target Responses

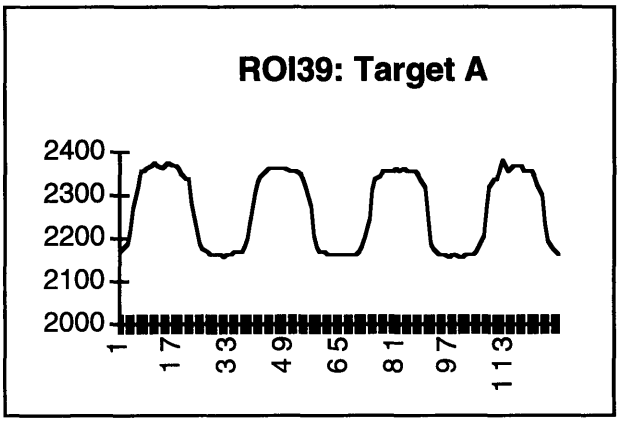

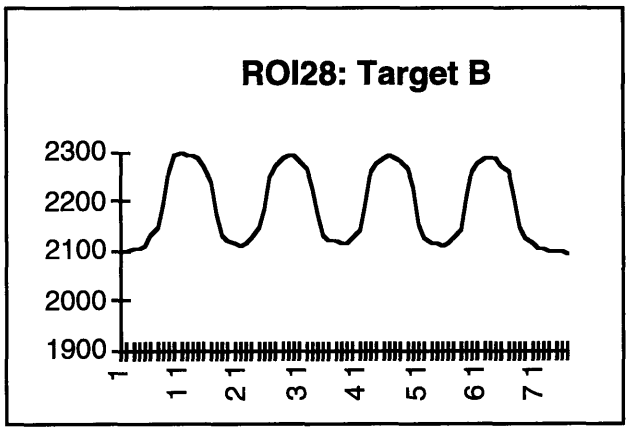

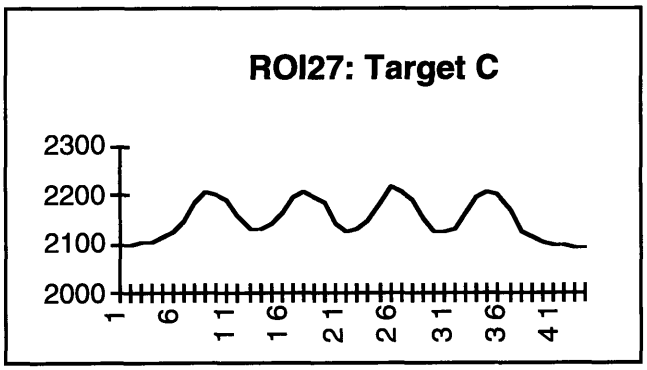

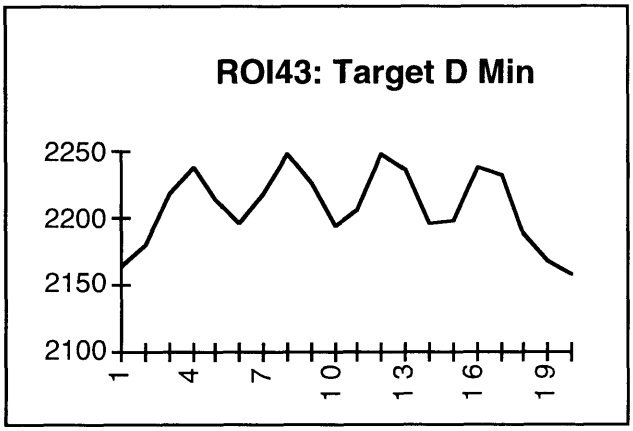
ROI43: Target D Min
2250
2200
2150
2100
1
4
7
10
13
16
19

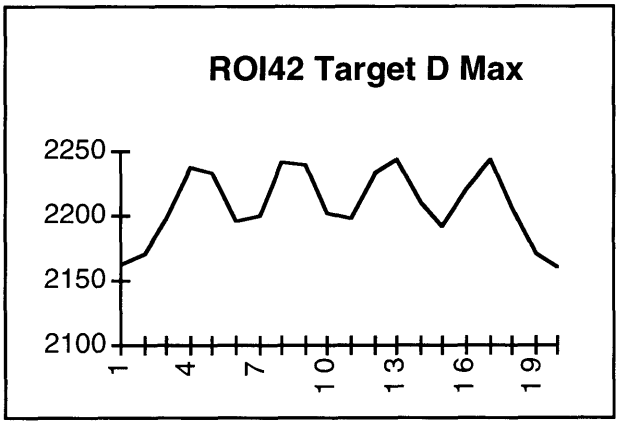
ROI42 Target D Max
2250
2200
2150
2100
1
4
7
10
13
16
19

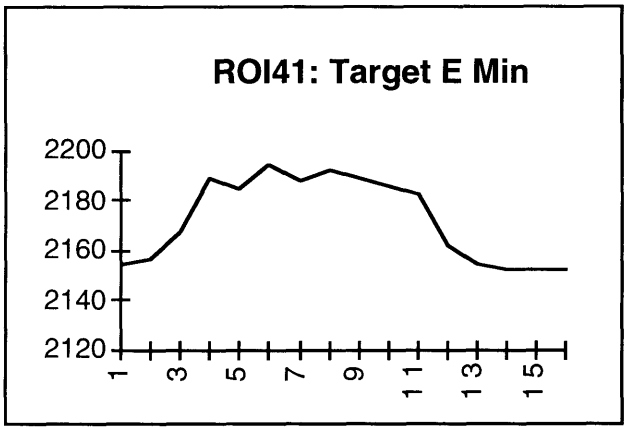
ROI41: Target E Min
2200
2180
2160
2140
2120
1
3
5
7
9
11
13
15

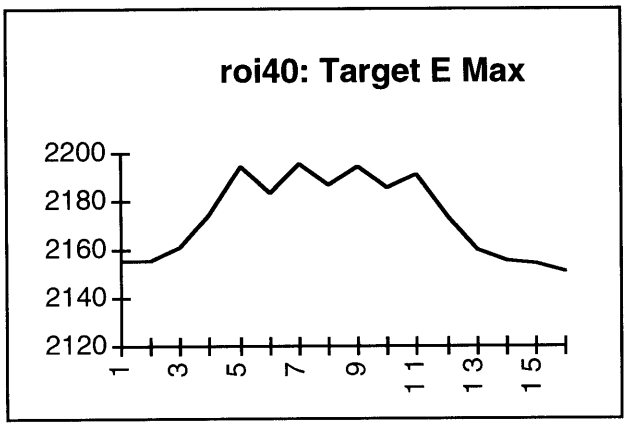
roi40: Target E Max
2200
2180
2160
2140
2120
1
3
5
7
9
11
13
15

Biographical Note

Howard Wexler is an alumnus of Rutgers Preparatory School of Somerset, New Jersey. He spent his undergraduate days at Tufts University in Medford, Massachusetts, obtaining his bachelor's degree in Electrical Engineering *cum laude* in 1989. Since 1988 he has been a member of Raytheon Company's Digital Systems Laboratory in Tewksbury, Massachusetts. His work at Raytheon has been in the field of signal and image processing. In 1993 he was awarded the Raytheon-MIT Masters in Industry Fellowship, which is awarded every two years to one recipient for graduate study at MIT.

Howard's extracurricular achievements include: President of Alpha Sigma Phi Fraternity, Beta Iota Chapter, Tufts University; Vice President, Dormitory Government, Tufts University; Chief Engineer, Tufts University Television; Private Pilot, single engine land airplane, instrument airplane. In addition, he enjoys equestrian sports, skiing, and fishing.